W-39

NATIONAL ADVISORY COMMITTEE FOR AERONAUTICS

WARTIME REPORT

ORIGINALLY ISSUED

February 1943 as
Advance Restricted Report

PRESSURE LOSS IN DUCTS WITH COMPOUND ELBOWS

By John R. Weske
Case School of Applied Science

NACA

WASHINGTON

NATIONAL ADVISORY COMMITTEE FOR AERONAUTICS

ADVANCE RESTRICTED REPORT

PRESSURE LOSS IN DUCTS WITH COMPOUND ELBOWS

By John R. Weske

SUMMARY

Results are presented of measurement of the pressure drop in ducts produced by two equal 90° elbows arranged at three different angular positions to each other, placed adjacent to each other, or separated by straight ducts of various lengths. The measured pressure drops have been analyzed and correlated, and the results are summarized in the form of curves adapted for design computations of pressure drop in compound-duct bends.

INTRODUCTION

A program of systematic investigation of the pressure drop and, in some cases, of the velocity distribution in compound elbows was undertaken for the purpose of furnishing to the designer of ducting systems in aircraft certain engineering data required for the computation of pressure losses in these systems. At the suggestion and with the financial support of the National Advisory Committee for Aeronautics, the work was undertaken at Case School of Applied Science. The design of the ducts, the testing, and the computation of the results was carried out by Frank E. Marble, J. J. Jacklitch, Jr., research assistants and Donald W. Steel, instructor at Case School of Applied Science.

APPARATUS AND EQUIPMENT

Testing Equipment

The layout of the test stand for the measurement of pressure drop in compound bends is shown in figure 1 and a photograph of the setup for a particular test is reproduced as figure 2.

Blower. - The equipment is powered by a type 35-20 North American centrifugal blower rated as follows:

Maximum speed, 3500 rpm

Quantity of flow, 5800 cubic feet per minute

Total pressure, 20 ounces per square inch

A measured performance curve of this blower at 3000 rpm is shown in figure 3.

The blower is driven by a direct-current motor that may be connected to either the 110-volt or the 220-volt direct-current laboratory circuit, thus affording speed control of great accuracy over a wide range and making it possible to extend the series of tests over a considerable range of Reynolds numbers. In a 6-inch-diameter duct, for instance, it is possible to attain Reynolds numbers of 1,000,000. Mach numbers are as high as 0.3.

Still larger Reynolds numbers may be obtained by placing a diffuser at the outlet of the duct and thereby recovering a sizeable portion of the kinetic energy of the stream. It has not been necessary to apply the diffuser for the present investigation because the capacity of the blower has been more than adequate.

Intake box and measuring orifice. - The intake box is 36 by 36 inches in cross section and 48 inches long. The rear face has a 23-inch-diameter opening with fairing in the box to change from square to round. The outlet opening of the box is placed tightly against the inlet opening of the blower, which has a diameter equal to that of the box.

The quantity of flow is measured at the inlet side of the blower by means of four exchangeable sharp-edge orifices mounted in the intake box. These orifices are symmetrically arranged on a circle about the axis of the box.

The diameters of the orifices are $4\frac{7}{16}$ inches, $7\frac{13}{16}$ inches, $6\frac{7}{64}$ inches, and $8\frac{7}{8}$ inches. Measurements of pressure drop are obtained by means of a tap in the side wall of the intake box, located on the horizontal center plane, 1 inch downstream of the orifices. The accuracy of quantity measurement should be ±1.5 percent according to reference 1.

The amount of leakage of air in the fan and the adjoining ducting was determined in a special test. In this test the outlet of the discharge ducting and the inlet were flanged off and, with the blower standing still, air was forced into this system by means of a vacuum-cleaner fan. The quantity of air handled by the vacuum-cleaner fan was determined for various static pressures produced in the system. The results of these measurements showed that under normal conditions of operation the amount of leakage, such as occurs at the shaft seal of the blower, would not appreciably affect the accuracy of measurement. Simultaneous determination of the quantity of flow from orifice measurements and from velocity-traverse measurements at the discharge of the plenum chamber gave results that agreed within 2 percent.

Plenum chamber. - Connected to the discharge opening of the blower there is a plenum chamber 48 inches long and $17\frac{1}{8}$ by $17\frac{1}{8}$ inches in cross section. A honeycomb section is mounted inside the plenum chamber 24 inches from the fan outlet. The sections of the honeycomb are 3/4 by 3/4 by 8 inches deep. Screen wire 18 mesh to the inch, 1/100-inch-wire diameter, is installed 10 inches downstream of the honeycomb to equalize the flow and further to reduce the turbulence. The maximum velocity in the plenum chamber is 30 feet per second. The plenum chamber is faired down to a cross section of shape and dimensions corresponding to those of the duct to be tested by a false structure extending 12 inches upstream from the outlet and a nozzle. The nozzle, 4 inches in length, connects the outlet of the plenum chamber to the duct and effects a gradual change of cross section to that of the duct. The contraction ratio of the transition from plenum chamber to duct is 10:1 for ducts of a cross-sectional area equal to that of a 6-inch-diameter duct.

Traversing head. - A traversing head and a multitube manometer (figs. 4 to 6) were used to obtain the velocity distribution in the 6-inch-diameter duct. Wall taps were used to get additional static-pressure measurements in the plane of the traverse. The traversing head also had a rake of silk threads for observation of the direction of flow through windows provided for the purpose. This rake is arranged at right angles to the tubes to minimize interference with the flow past the tubes. The traversing head can be rotated between its flanges to obtain a number of diametral traverses. Records of pressure distribution were obtained by blueprinting the shadow of the meniscuses.

Ducts and Elbows

The straight ducts used in these tests of round and elliptical cross section were made of galvanized iron. They were joined together with flanges made of 3/4-inch plywood. The straight ducts of square and rectangular cross section were made of white pine and plywood, which was varnished on the inside to close the pores and decrease the roughness. These ducts were also provided with flanges. Precise alinement was obtained by insertion into the flanges of brass dowels, such as are used in patternmaking. By this means deviation from alinement of the inside walls is kept below 1/32 inch. Preliminary tests of both the elliptical and rectangular ducts of large aspect ratio disclosed that they would distort under internal pressure. In order to prevent this distortion, frames were mounted around the ducts at intervals of 12 inches and the correct cross section was thereby maintained, within close limits, over the entire length of the duct.

The elbows of round and elliptical cross section were carved to templet from glued blocks of wood. Their inside surface was rendered smooth by two coats of shellac, of which the first one was rubbed down before application of the second. The three single elbows of circular cross section are shown in figure 7. The elbows of square and rectangular cross section were made of galvanized iron and were provided with flanges on both ends. (See fig. 8.) The seams were such that they left the inside perfectly smooth. These elbows, as well as the ducts of square and rectangular cross section, had sharp corners without fillets. Dimensions of the elbows are given in table I.

TABLE I

DIMENSIONS OF ELBOWS

Elbow	Cross section	Width / Depth	Dimensions (in.)	Area (sq. in.)	Mean radius (in.)	Radius ratio
1 2 3	Circular	1	Radius 3	28.2	4.5 9.0 24.0	0.75 1.5 4.0
4 5 6	Elliptical	3	Major axis 10.5 Minor axis 3.5	28.2	2.65 5.25 14.0	0.75 1.5 4.0
7 8 9	Elliptical	5	Major axis 13.25 Minor axis 2.65	28.2	2.0 4.0 10.6	0.75 1.5 4.0
10 11 12	Square	1	Width 5.125 Depth 5.125	28.0	3.9 7.75 20.75	0.75 1.5 4.0
13 14 15	Rectangular	3	Width 9.1875 Depth 3.06	28.0	2.3 4.6 12.25	0.75 1.5 4.0
16 17 18	Rectangular	5	Width 11.875 Depth 2.375	28.0	1.8 3.56 9.5	0.75 1.5 4.0

At the cross sections of the straight duct, selected for static-pressure measurements, four pressure taps were located in the same transverse plane. In the case of the round ducts, the wall taps were spaced equally around the circumference. In the ducts of elliptical cross section, taps were provided on the major and minor axes - one on each side. For ducts made of galvanized iron, these taps were drilled with a No. 40 drill. In the case of ducts made of wood a thick-wall brass tube with a 1/32-inch-diameter hole was inserted in the wall, filed flush with the inside surface. Burrs were carefully removed and, in the case of the wooden ducts, pattern wax was applied in crevices to insure a perfectly smooth and regular surface in the vicinity of the pressure tap. The four pressure taps were interconnected by a circular line from which one connection was led to a U tube.

Photographs of the test setup for a U bend of the 5 x 1 rectangular duct and for a 90°-offset bend of the 5 x 1 elliptical duct are shown in figures 9 and 10, respectively. The photograph, figure 9, was taken before stiffening frames were applied, while figure 10 shows the stiffening frames. In the case of the 90°-offset bends of the elliptical and rectangular ducts the inlet area of the second elbow was angularly displaced by 90° with respect to the outlet area of the first elbow. (See fig. 10.) The transition was accomplished by means of two transition sections, each 1 foot long, changing the elliptical section into a circular section of the same area and, correspondingly, the rectangular section into a square section of the same area. One transition section was placed directly downstream of the second elbow. The required length of spacer was produced by placing a piece of duct of circular (or square) section between these two transition pieces. For minimum length of spacer, the two transition pieces were placed flange to flange.

CALIBRATIONS

Calibration tests of the blower, in which the speed was held constant and the air was discharged against resistances of the order of magnitude to be encountered in the ducting, had shown that the testing equipment has ample capacity. A characteristic performance curve of the blower at 3000 rpm is shown in figure 3. The electrical equipment was chosen to permit very sensitive speed control and, at the same time, to keep an established condition of operation constant for the duration of the run.

As previously stated, quantity measurements computed from orifice- and velocity-traverse measurements agreed within 2 percent. This agreement was accepted as satisfactory.

Preliminary to the determination of coefficients of friction of the straight duct, tests were conducted to establish the effect of approach length, that is, the length of duct required to produce a fully developed velocity profile. It might be expected that in the approach length the pressure gradient is larger than the pressure gradient in the part of the duct in which the profile is fully developed. Evidence was obtained from velocity traverses and pressure measurements that the boundary layer developed very rapidly immediately downstream of the nozzle and more slowly with increasing distance from the nozzle, thus approaching asymptotically the fully developed state.

The friction drop in a 6-inch-diameter straight duct of circular cross section was determined for a 30-foot length between taps, beginning 4 feet from the nozzle, and for a 20-foot length between taps, beginning 14 feet from the nozzle. It was observed, however, that it was more difficult to obtain consistent pressure readings on the upstream taps with the shorter approach length than with the longer. On the basis of these tests, the rule was established of running pressure-drop tests with a straight approach length at least 15 hydraulic diameters long ahead of the upstream pressure tap. In the case of the round duct, the approach length was 28 diameters.

Exploratory measurements of velocity distribution showed that in order to obtain a symmetrical velocity profile in the straight duct it was imperative to aline the duct carefully. Slight bends in the duct would affect the velocity pattern considerably. Care was therefore taken in all tests that the duct sections were lined up straight with each other and with the nozzle.

Velocity traverses were taken for the duct of circular cross section at the outlet of the nozzle (fig. 11) and at a point in the straight duct 28 diameters downstream of the nozzle, which corresponds to the location of the inlet of the first elbow in the elbow tests (fig. 12). The straight duct was continued 20 diameters downstream when it opened into atmosphere. Figure 12 shows the velocity patterns with test points plotted for various speeds.

TESTS

The tests deal with three principal aspects of the investigation, namely,

1. The determination of friction coefficient for the straight duct

2. The measurement of pressure drops of single elbows

3. The measurement of pressure drops of compound elbows in three different arrangements, referred to as Z-bend, U-bend, and 90°-offset bend, as indicated in figure 1

Some measurements were made of the velocity distributions in the separated regions downstream of the single circular elbows. Additional qualitative measurements of the velocity fluctuations in these regions were made with a hot wire and an oscillograph. Velocity and stream-angle surveys were also made at the outlet of a compound bend in a circular duct. The tests were made at mean air velocities in the duct of 100, 200, and 300 feet per second and at lower and intermediate speeds when necessary. These velocities covered a Reynolds number range from 2×10^5 to 8×10^5 for the circular duct and a corresponding range of slightly lower Reynolds numbers for the other ducts because of their lower hydraulic diameter.

The pressure drop of the single and compound bends was measured by means of static-pressure orifices 1 foot upstream of the inlet of the first elbow and 4 feet downstream of the outlet of the second elbow, except for the single elbows of circular cross section, for which the downstream pressure tap was only 2 feet from the outlet of the elbow.

In addition to the readings necessary for the determination of quantity of flow and of pressures, it was found necessary to measure air temperatures both on the inlet side and the discharge side of the blower; there was a considerable temperature increase, particularly for duct arrangements of high resistance.

SYMBOLS

f	friction factor of straight duct at Reynolds number R of test
R	Reynolds number $(\rho Vd/\mu)$
V	mean velocity in the duct
ρ	mass density at temperature and pressure of air at blower outlet
μ	absolute viscosity at temperature and pressure of air at blower outlet
Δp	measured pressure drop between taps
$\Delta p'$	net pressure drop
q	dynamic pressure $\left(\frac{1}{2}\rho V^2\right)$
L'	developed length between inlet flange of first elbow and outlet flange of second elbow
l_1	distance of upstream pressure tap from inlet flange of first elbow
l_2	distance of downstream pressure tap from outlet flange of second elbow
l	length of straight duct between upstream and downstream elbows
r	radius of curvature of center line of elbow
d	hydraulic diameter of duct $\left(\frac{4 \times \text{area}}{\text{perimeter}}\right)$
L	distance between inlet and outlet ducts of compound elbow $(L = l + 2r)$
A	cross-sectional area of duct

RESULTS

Pressure Loss in Straight Ducts

The results of measurements of the pressure drop of the straight duct are presented in figure 13 for ducts of all cross sections tested.

This graph shows coefficients of friction f

$$f = \frac{\Delta p}{q} \frac{d}{l}$$

based on the hydraulic diameter d, plotted against Reynolds number. It is seen that, when correlated by means of the hydraulic diameter, the friction coefficients of all cross sections investigated do not differ much; it is therefore possible to draw a curve through the test points that may then be applied with close approximation to round and elliptical as well as to square and rectang lar cross sections. The curve lies slightly above the von Kármán-Nikuradse curve (see reference 2, p. 144) for smooth round tubes.

Pressure Losses in Single and Compound Bends

For presentation of results, the measured pressure drop Δp was reduced to nondimensional form through division by the dynamic pressure q. The quantity $\frac{\Delta p}{q}$ represents the nondimensional gross pressure drop. Next, a net pressure drop $\Delta p'$ was computed by deducting from the measured pressure drop corresponding to the friction loss of a straight duct of length equal to the developed length of the duct between the two pressure taps. Reduced to nondimensional form, the net pressure drop is thus defined as

$$\frac{\Delta p'}{q} = \frac{\Delta p}{q} - f\left(\frac{l_1 + l_2 + L'}{d}\right)$$

The values of $\Delta p'/q$ for all ducts have been plotted against Reynolds number in figures 14 to 25, where, to avoid confusion, the experimental points have been omitted from most of the curves. The scale effect appears to be slight for the round

and square ducts; for the ducts of high aspect ratio, however, the pressure drops tend to increase with increasing Reynolds number (figs. 19 and 25). In some cases (for example, fig. 15), the pressure drop showed a sharp rise toward the lowest Reynolds numbers; the data are not sufficient, however, to prove the existence of a critical Reynolds number in this range.

The results have been cross-plotted in figures 26 to 28 to show the effect of length of spacer between elbows. The values of $\Delta p'/q$ shown in these curves are the averages for the Reynolds number range tested, except for those cases in which the scale effect was unusually large, in which case curves for the high and low range are shown separately. (See figs. 27(c) and 28(c).) It is clear from these plots that the relative radius of curvature r/d is the most important of the factors affecting the net pressure drop. As compared with this factor the effect of length of spacer between elbows may be regarded as being of the nature of an interference. In general, as the length of the spacer is decreased, this interference causes a decrease of net pressure drop in the case of the U-bend (fig. 24), an increase in the case of the Z-bend (fig. 25), and almost no change in the case of the 90°-offset bend (fig. 26).

For the purpose of pointing out the relationship between the radius ratio of the elbows $\frac{r}{d}$ and the net pressure drop $\frac{\Delta p'}{q}$, a plot has been made in figure 29 of the net pressure drop $\frac{p'}{q}$ for the maximum length of spacer tested against the inverse of the radius ratio squared $\left(\frac{d}{r}\right)^2$ for ducts of all cross sections. This quantity was chosen as it was surmised that, in the absence of separation, there might possibly be proportionality between the net-pressure drop and the pressure gradient in the radial direction at the elbow. Inasmuch as such reasoning is crude from considerations of the nature of the physical phenomena, the quantity $\left(\frac{d}{r}\right)^2$, though not quite proportional to the pressure gradient, was considered adequate as a first approximation.

For the purpose of adapting the results of the experimental investigation for use in connection with the estimation of pressure drops in compound duct bends, 3 charts, figures 30, 31, 32 were prepared for the Z, U, and 90°-offset bends, respectively. On these charts were plotted the net pressure drops of compound bends of all ducts investigated against the quantity $\frac{r}{\sqrt{A}}$. These graphs show a family of curves for each duct section with the nondimensional normal distance between the axes of the upstream and downstream ducts $\frac{L}{\sqrt{A}}$ as parameters. The families of curves relating to the various duct sections have been plotted on one graph in order to facilitate comparison. Logarithmic paper was chosen for these plots not because of any inherent quality of the functional relations, but because it was felt that the accuracy of presentation was improved thereby.

Figure 33 shows the velocity traverses taken at the outlet in the symmetry plane of the single elbows. Only the sharpest bend shows complete separation from the inner wall. A map showing the velocities at 4 diameters in this section is given in figure 34. Owing to the pronounced fluctuation in the regions of separation (or of incipient separation), the velocities measured here exceed the two average velocities in the axial direction.

Some indication of the degree of fluctuation was afforded by the hot-wire measurements. Thus, figure 35, the ordinates of which are proportional to the mean local airspeed, shows a different distribution from that of the corresponding curve of figure 33. Oscillograms taken in the "separation" inner region and the "smooth" outer region are compared in figure 36.

Figure 37 shows surveys of velocities, static pressure, and angles of flow at the outlet of a 90°-offset compound bend. The variation in angle of flow across the duct indicates a pronounced rotation of the flow. The fact that the net pressure drops of the 90°-offset bends are lower than those of the U-bend and Z-bend may be traced to the effect of this rotation of flow in, and downstream of, the second elbow, which tends to energize the boundary layer.

CONCLUSIONS

1. Friction-drop coefficients of straight ducts, if computed on the bases of hydraulic diameter, are nearly independent of cross-sectional shape.

2. The pressure-drop coefficients for single and compound bends vary but slightly with Reynolds number in the range of Reynolds numbers from 2×10^5 to 8×10^5. The variation does not appear to be uniform.

3. The radius ratio is the most important of the variables for the three types of bend affecting the pressure-drop coefficient of bends.

4. For compound bends, the net pressure drop decreases with decrease of spacer length in the case of U-bends, and increases with decrease of length of spacer in the case of Z-bends. The effect of spacer length is very small in the case of the 90°-offset bends.

5. There is a rotation of the flow downstream of the 90°-offset compound bend. This rotation probably accounts for the fact that the pressure drops across the 90°-offset bends are less than those across the corresponding U-bends or Z-bends.

Case School of Applied Science,
Cleveland, Ohio.

REFERENCES

1. Marks, L. S.: Square Edged Inlet and Discharge Orifices for Measuring Air Volumes in the Testing of Fans and Blowers. A.S.M.E. Trans. AER 58-7, vol. 58, no. 8, Nov. 1936, pp. 593-597.

2. Prandtl, L.: Turbulent Flow along a Wall with Special Reference to the Frictional Resistance of Plates. Vol. III, div. G, Sec. 23 of Aerodynamic Theory, W. F. Durand, ed., Julius Springer (Berlin), 1935, pp. 145-154.

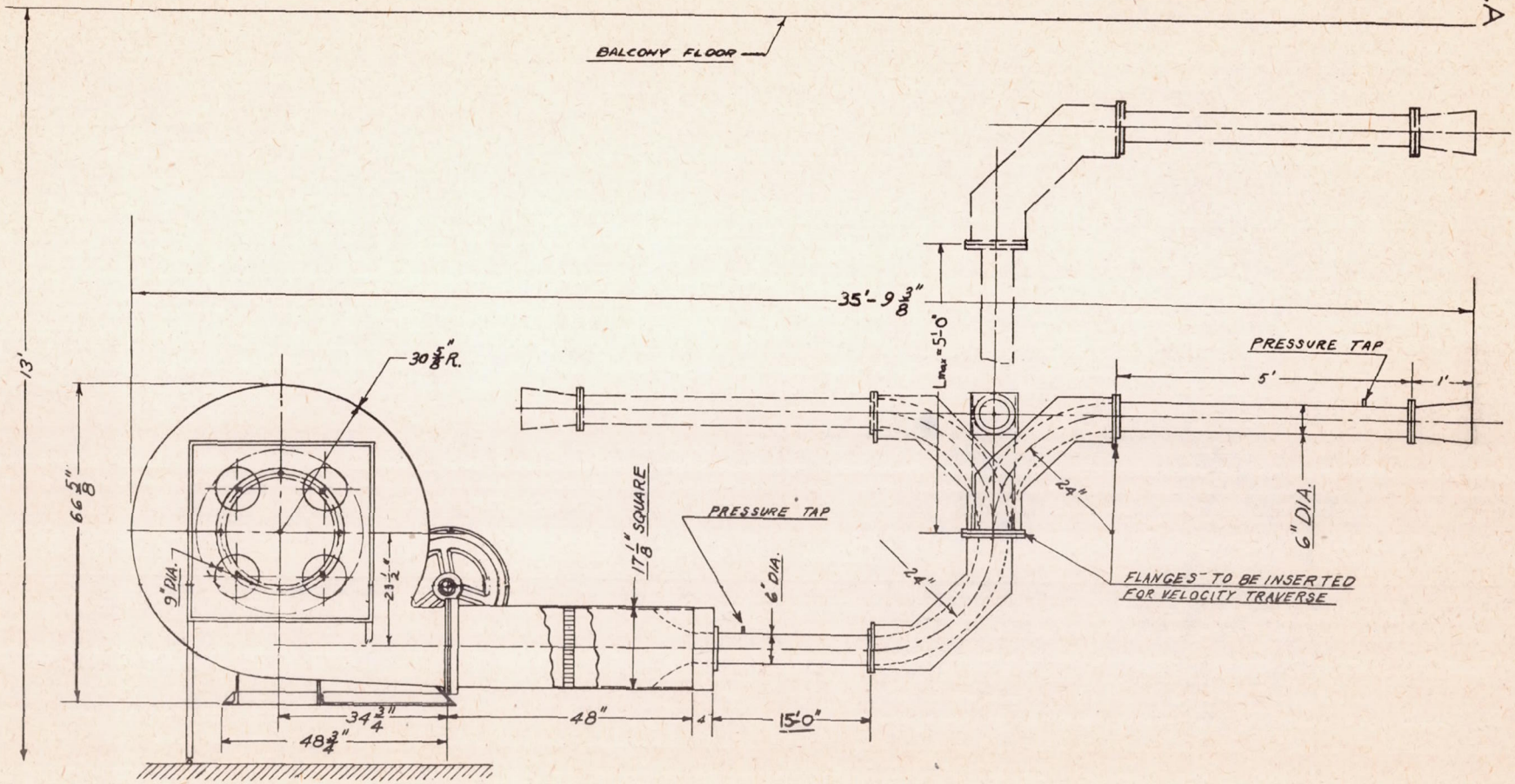

Figure 1(a,b).- Drawing of test set-up.

NACA

Fig. 1b

W-39

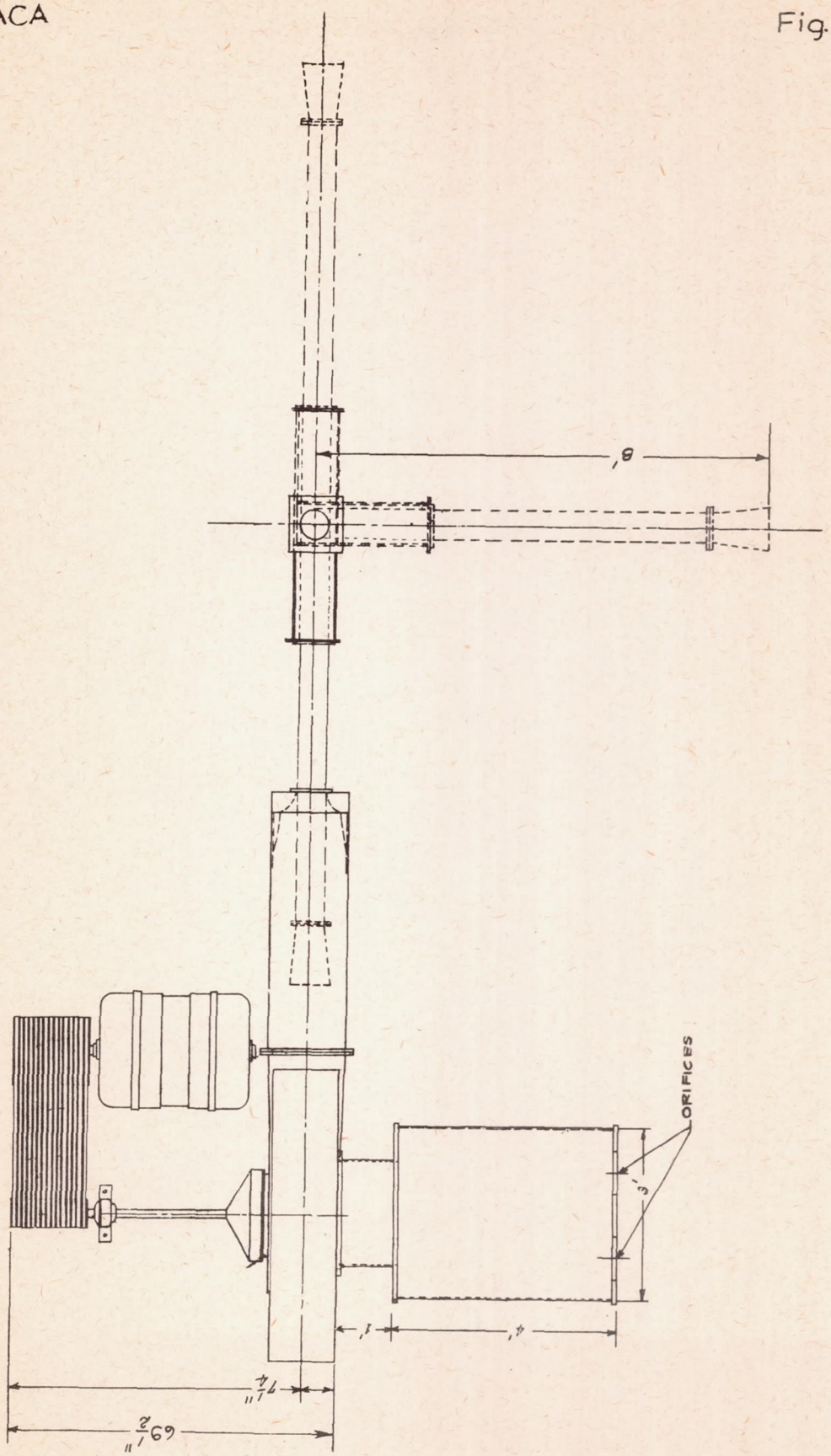

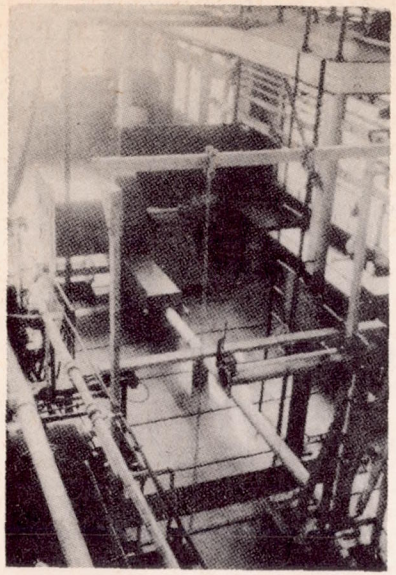

Figure 2.- Photograph of test set-up.

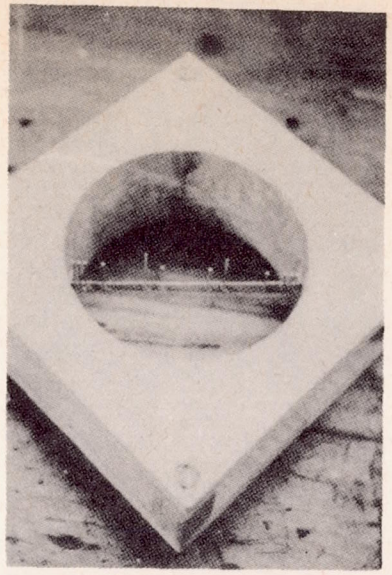

Figure 4.- Traversing head.

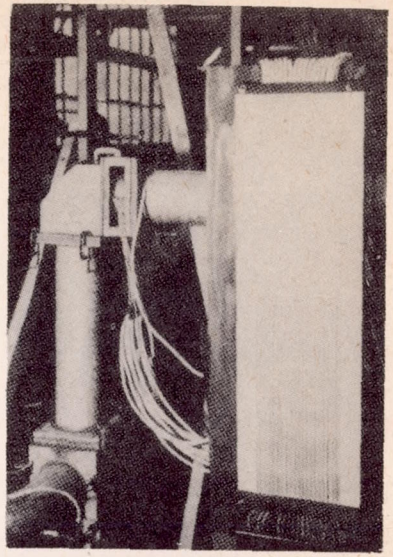

Figure 5.- Duct installation for test of 90° offset bend showing traversing head and multiple tube manometer.

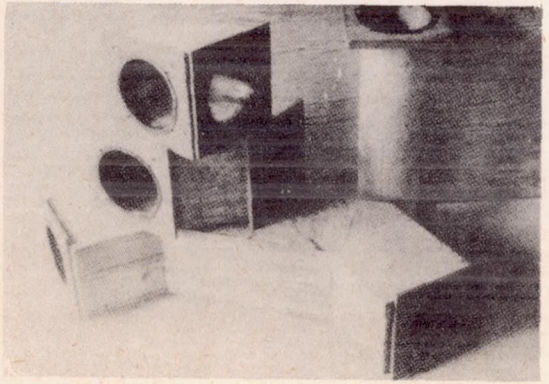

Figure 7.- Elbow and dust spacers of circular cross section.

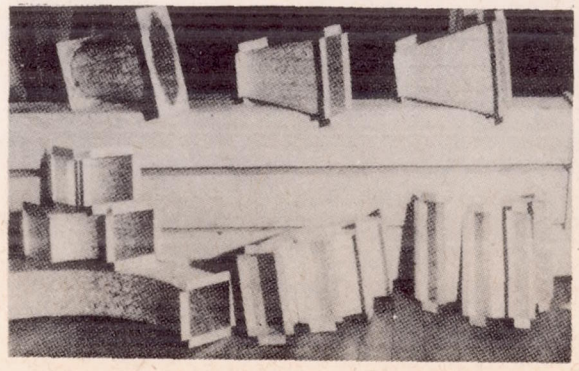

Figure 8.- Bends for rectangular ducts and outlets.

NACA

Figs. 2,4,5,7,8

W-39

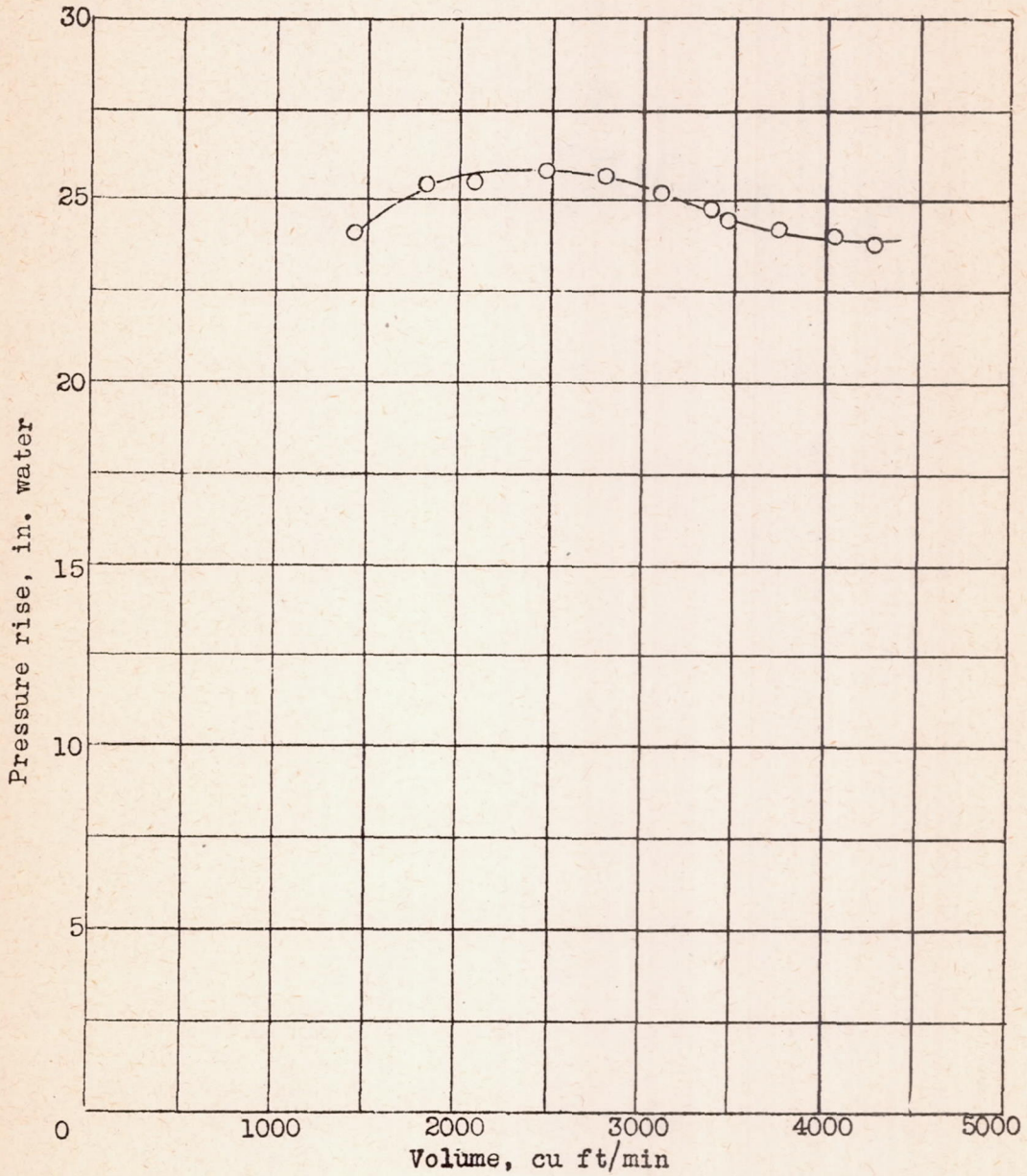

Figure 3.- Performance characteristics of blower at 3000 rpm.

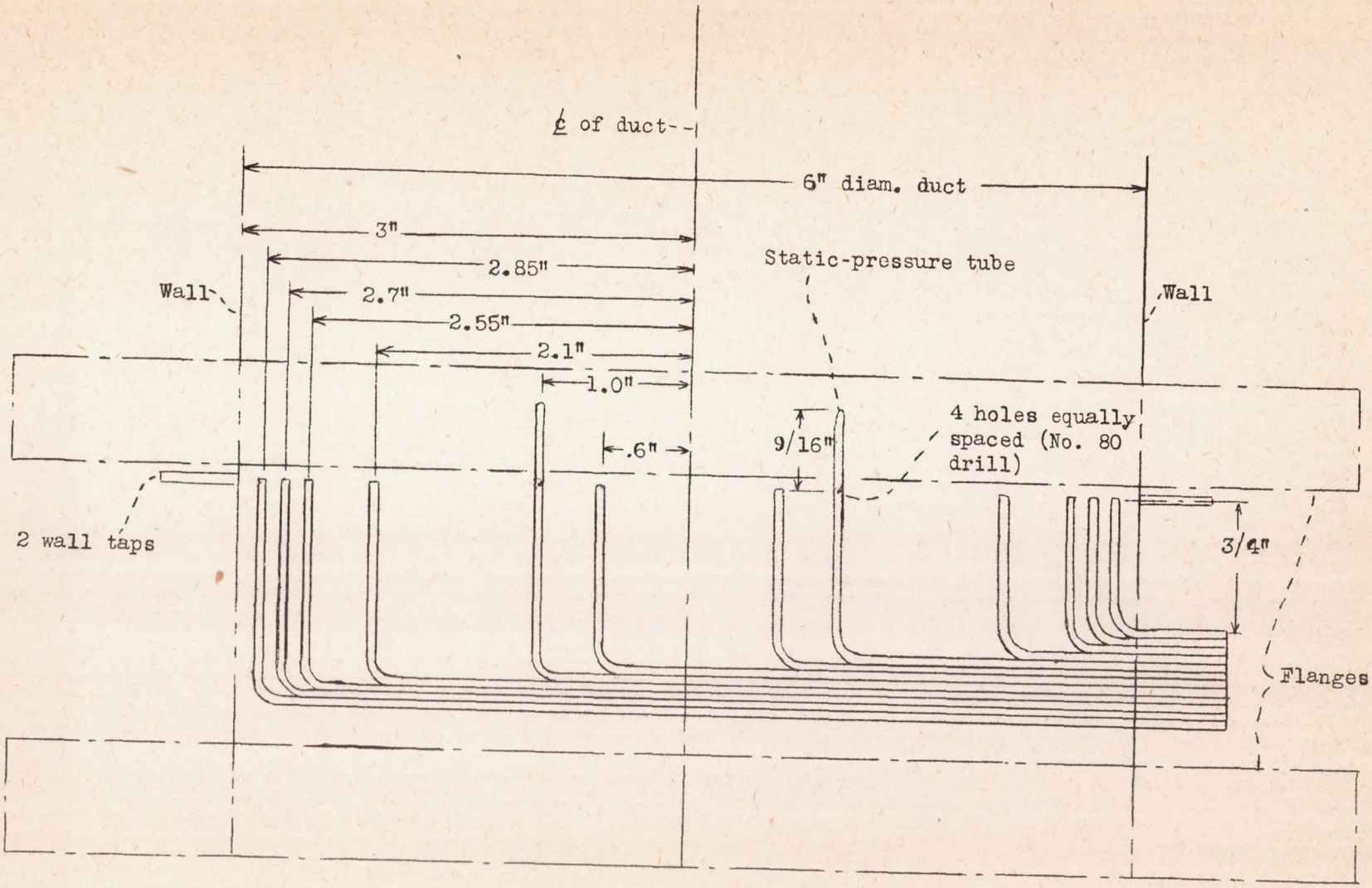

Figure 6.- Location of total- and static-pressure tubes of traversing head.

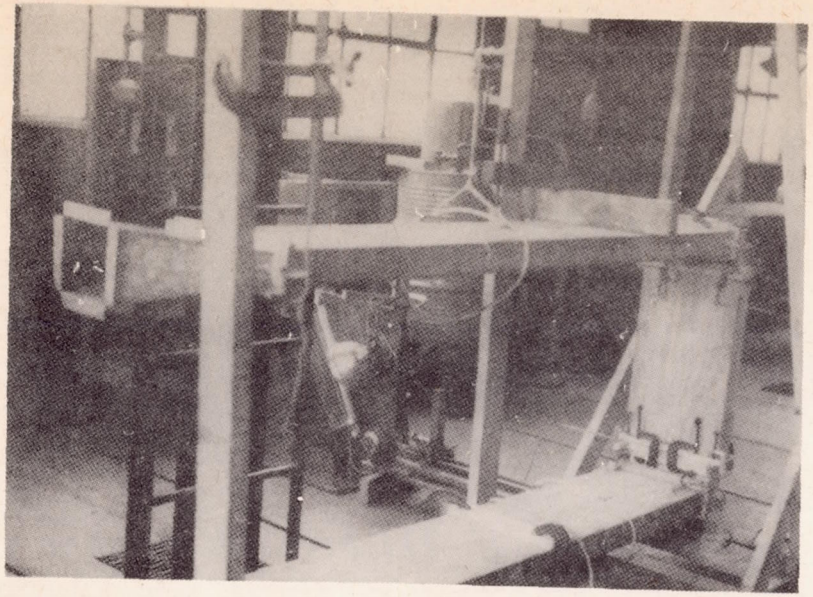

Figure 9.- Compound U-bend for rectangular duct.

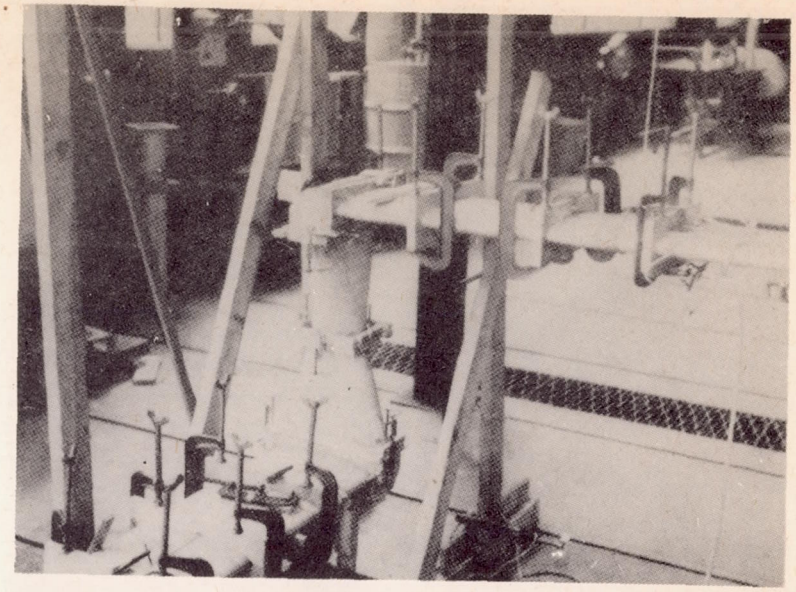

Figure 10.- Compound 90°-offset bend for elliptical duct.

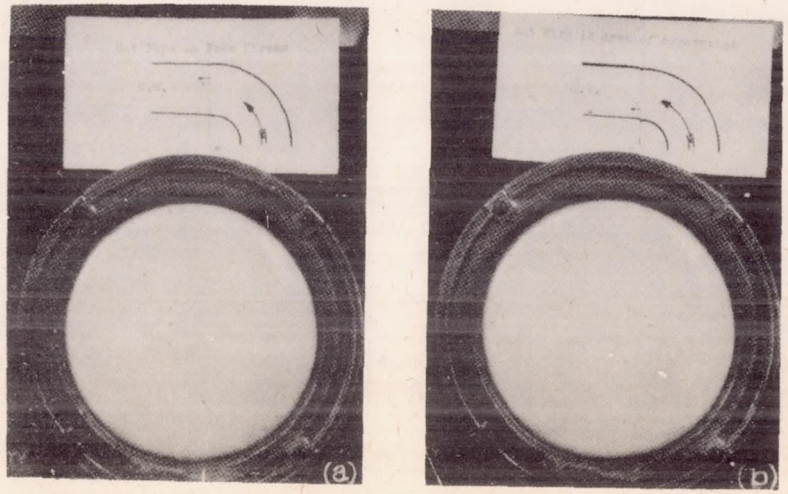

Figure 36.- Oscillogram showing speed fluctuations.

(a) In free stream.

(b) In area of separation.

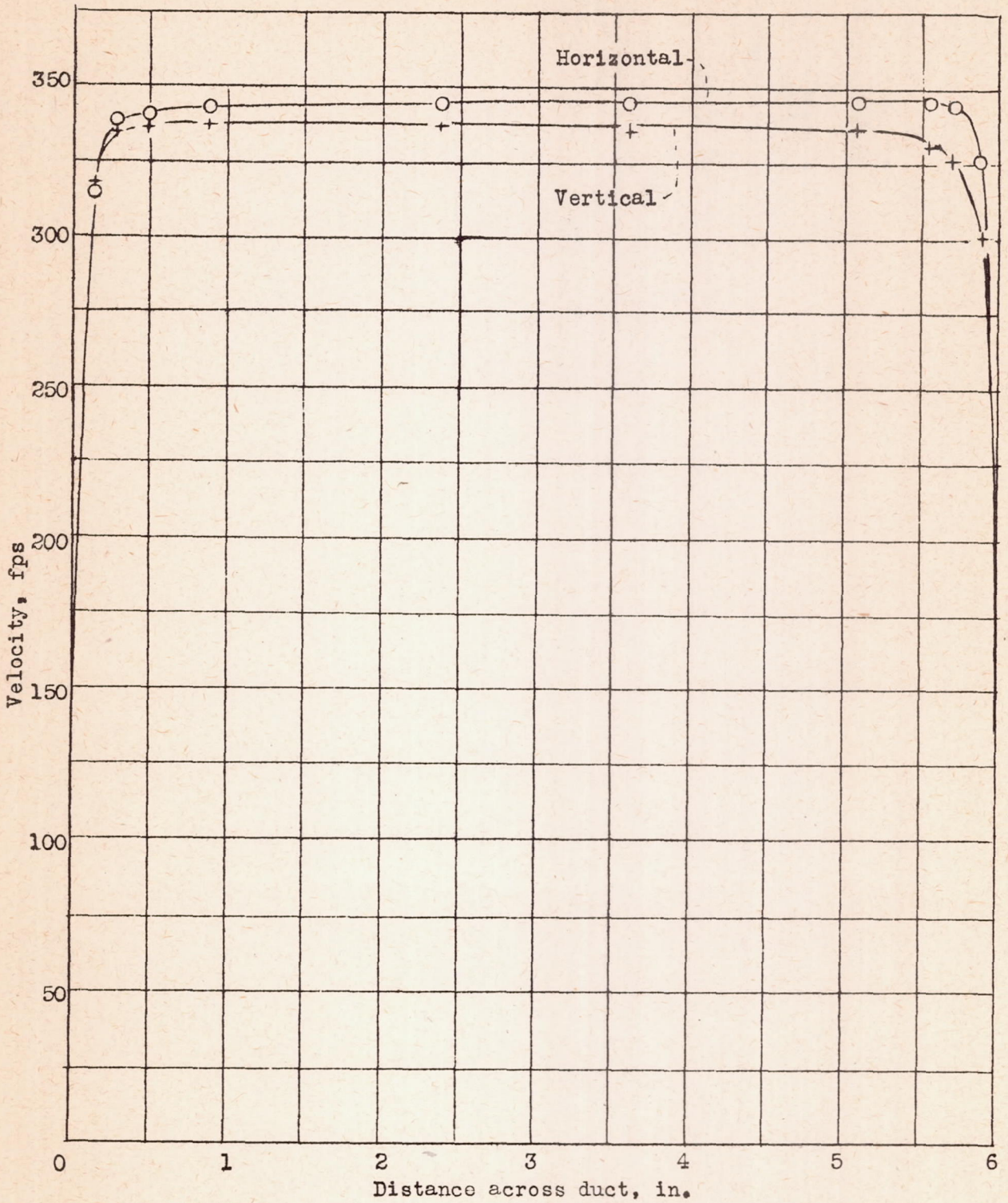

Figure 11.- Velocity traverse at the outlet of the 6-inch-diameter nozzle.

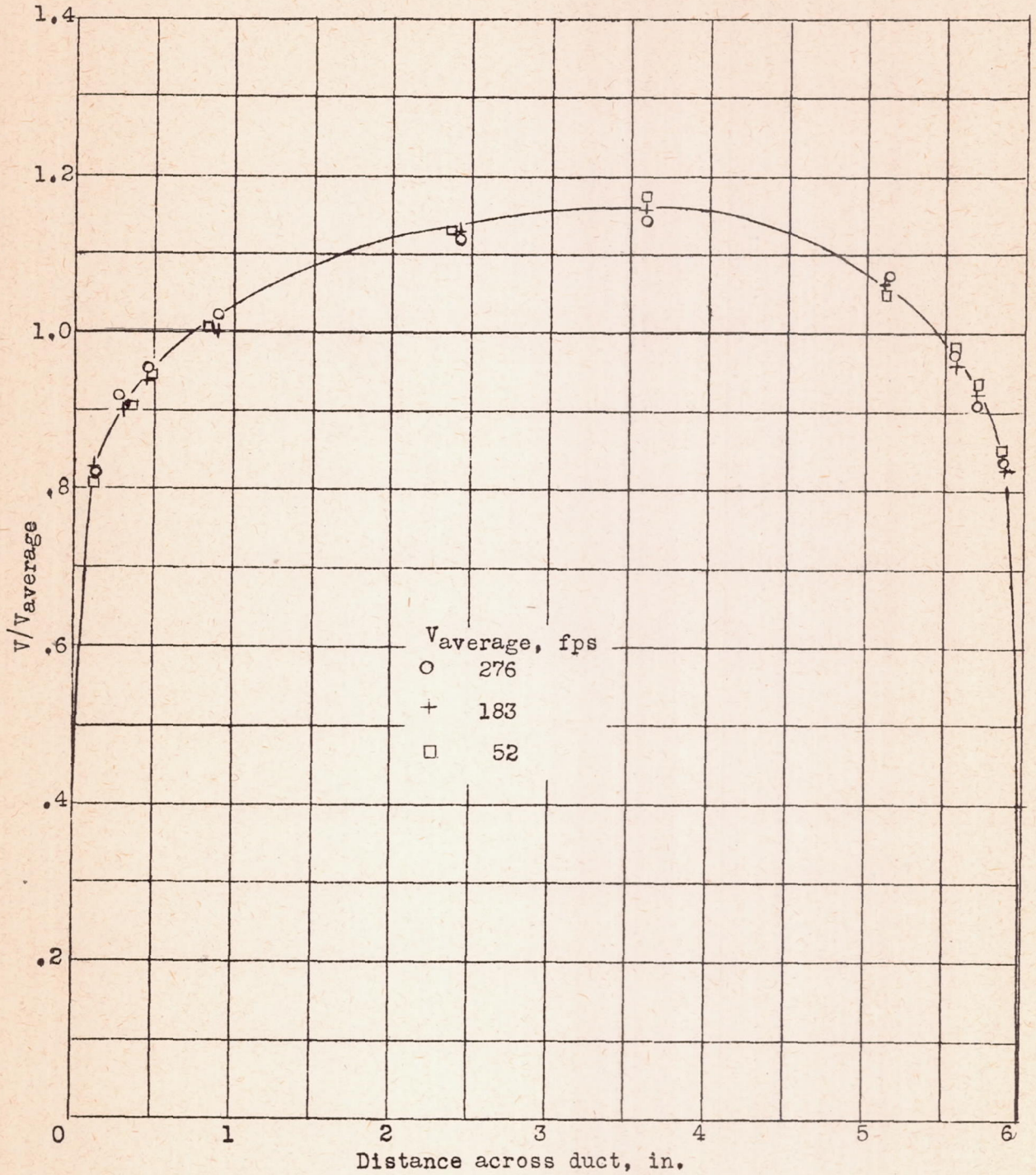

Figure 12.- Velocity traverses at inlet of the first elbow.

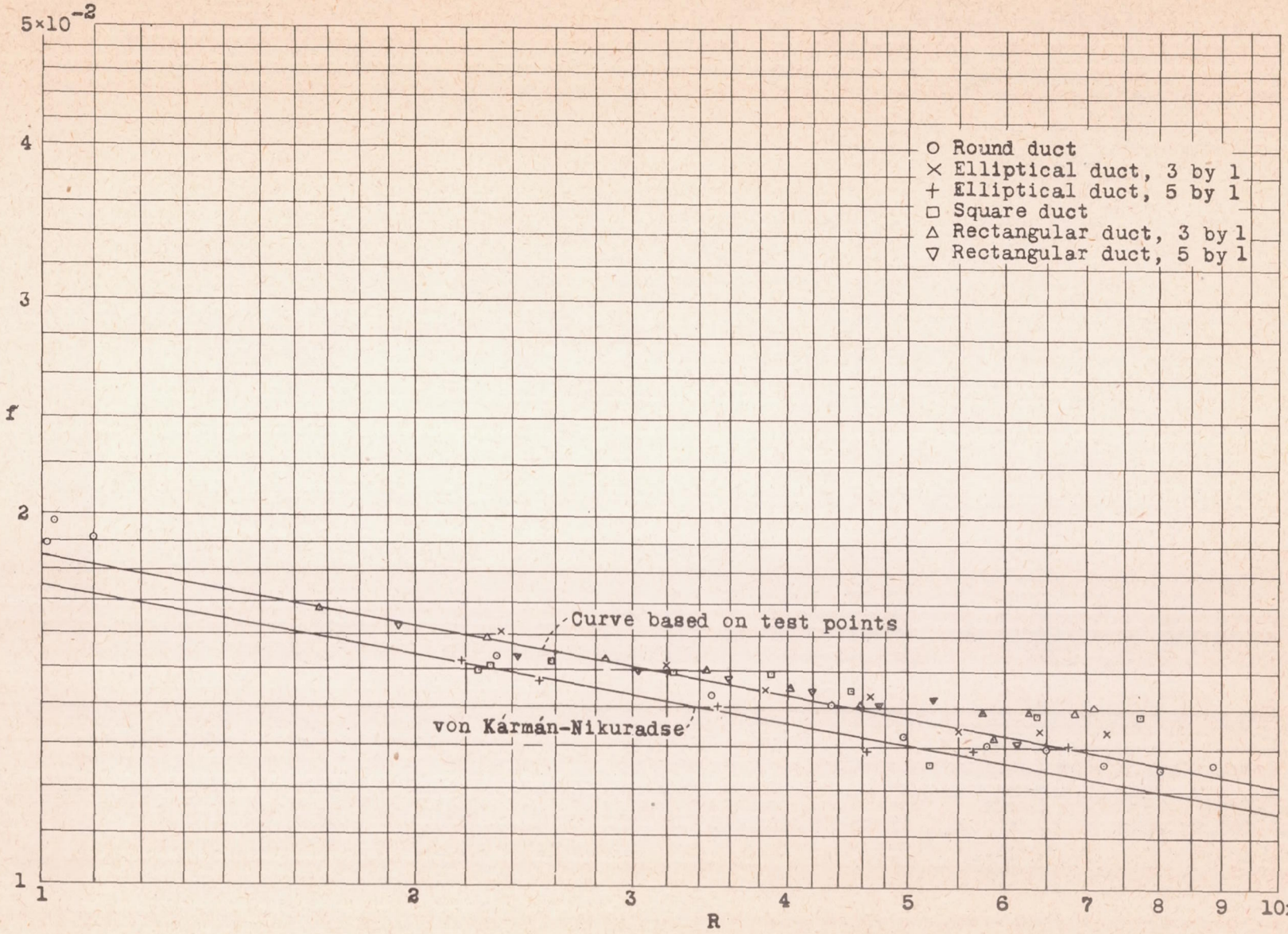

Figure 13.- Friction factor f against Reynolds number for ducts of various cross sections.

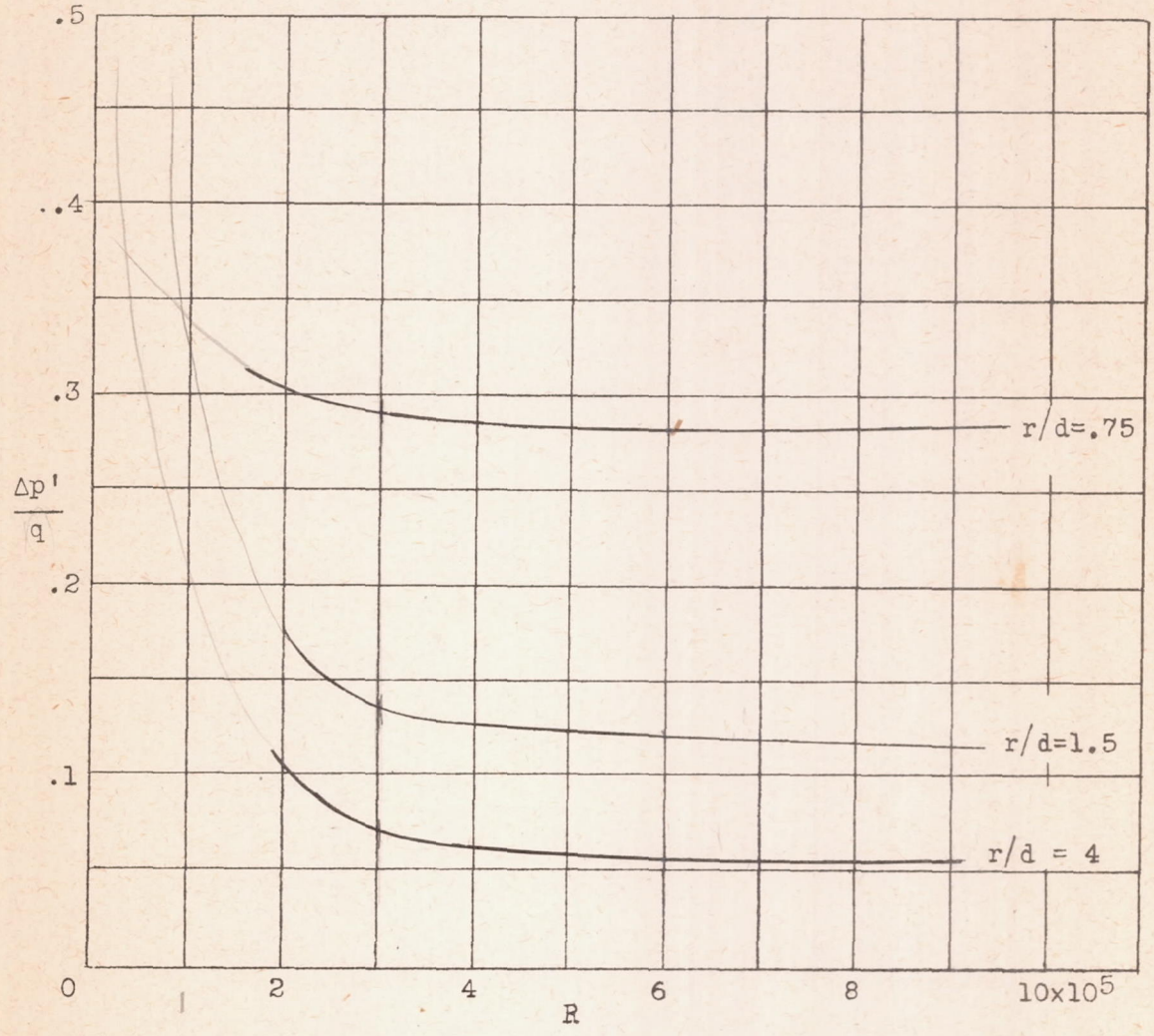

Figure 14.- Variation of net pressure drop with Reynolds number for single bends in circular ducts.

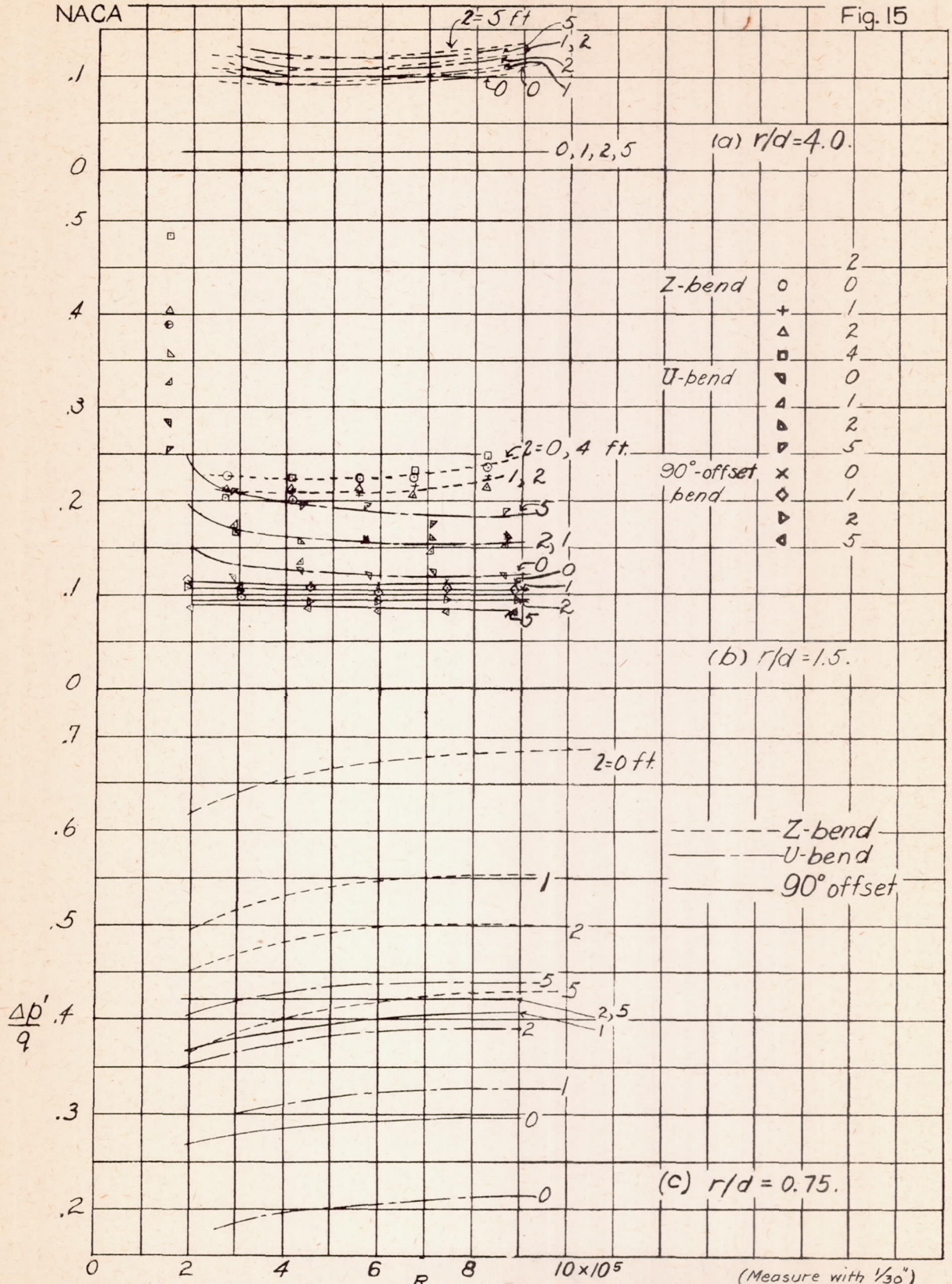

Figure 15.- Variation of net pressure drop with Reynolds number for compound bends in circular ducts.

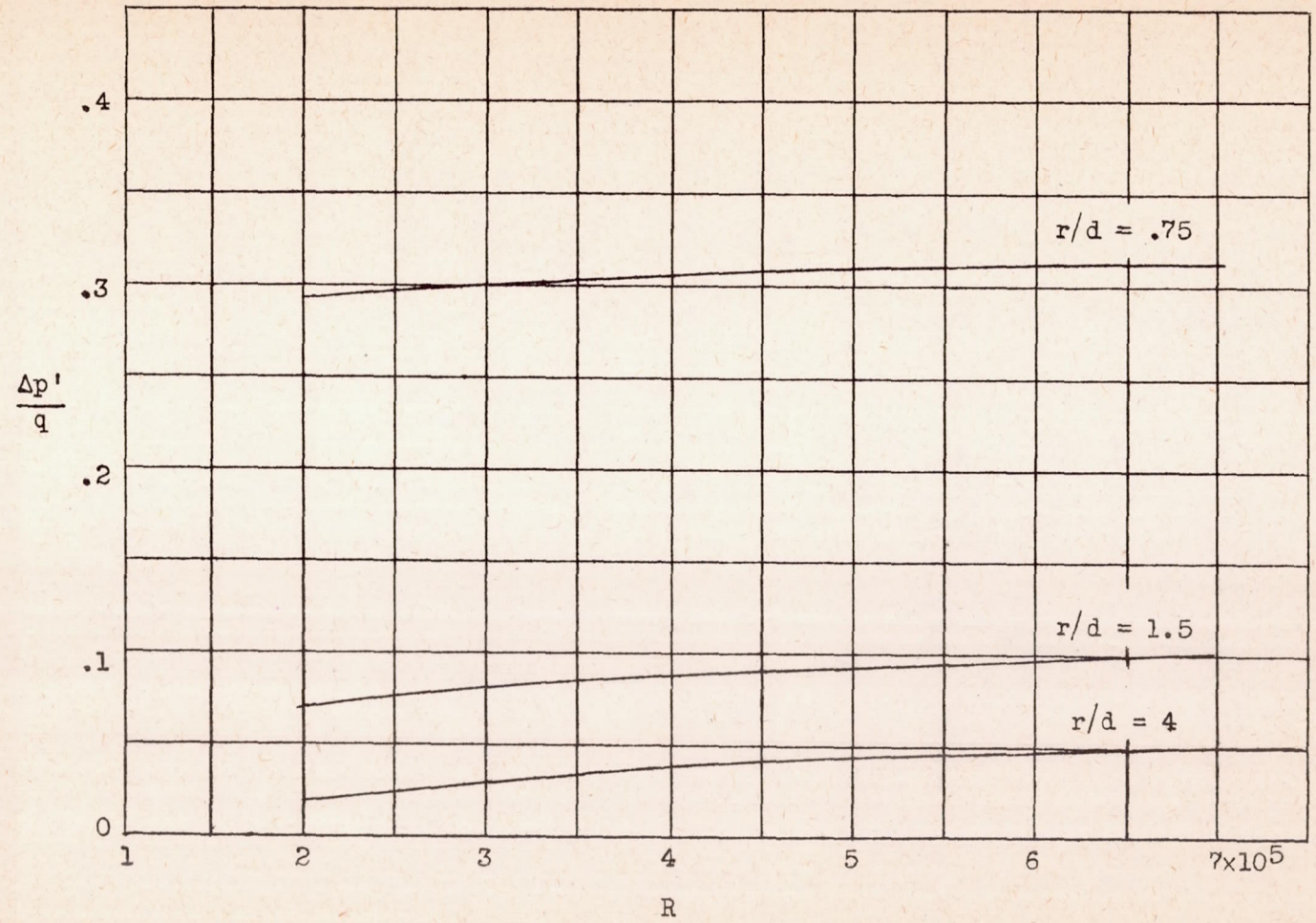

Figure 16.- Variation of net pressure drop with Reynolds number for single bends in 3 by 1 elliptical ducts.

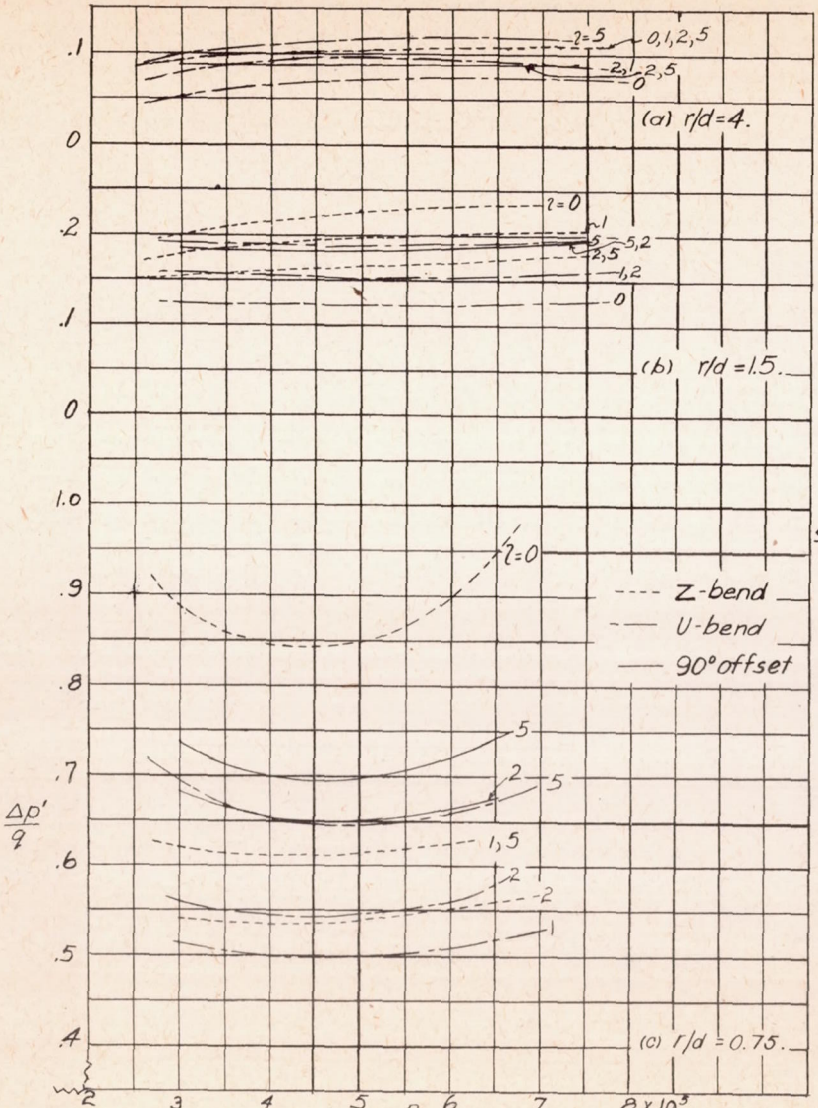

Figure 17.—Variation of net pressure drop with Reynolds number for compound bends in 3 by 1 elliptical ducts.

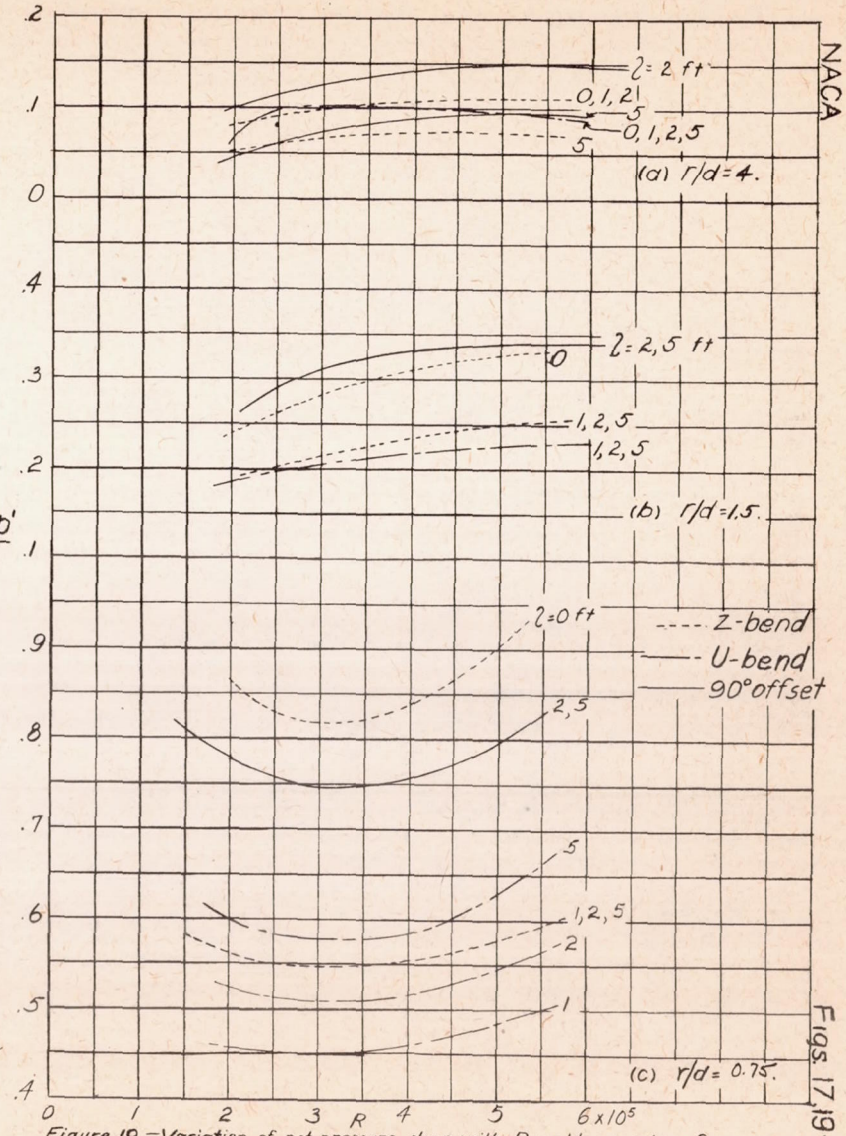

Figure 18.—Variation of net pressure drop with Reynolds number for compound bends in 5 by 1 elliptical ducts.

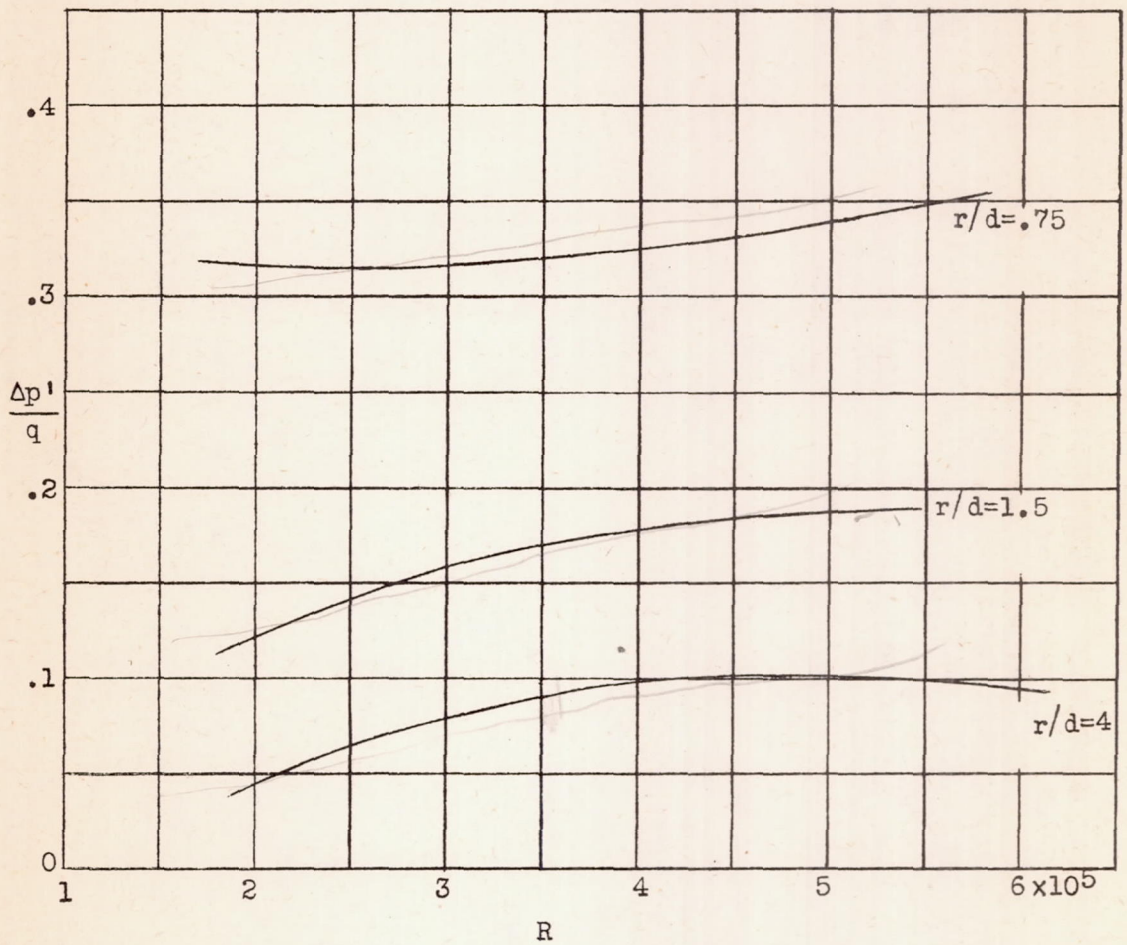

Figure 18.- Variation of net pressure drop with Reynolds number for single bends in 5 by 1 elliptical ducts.

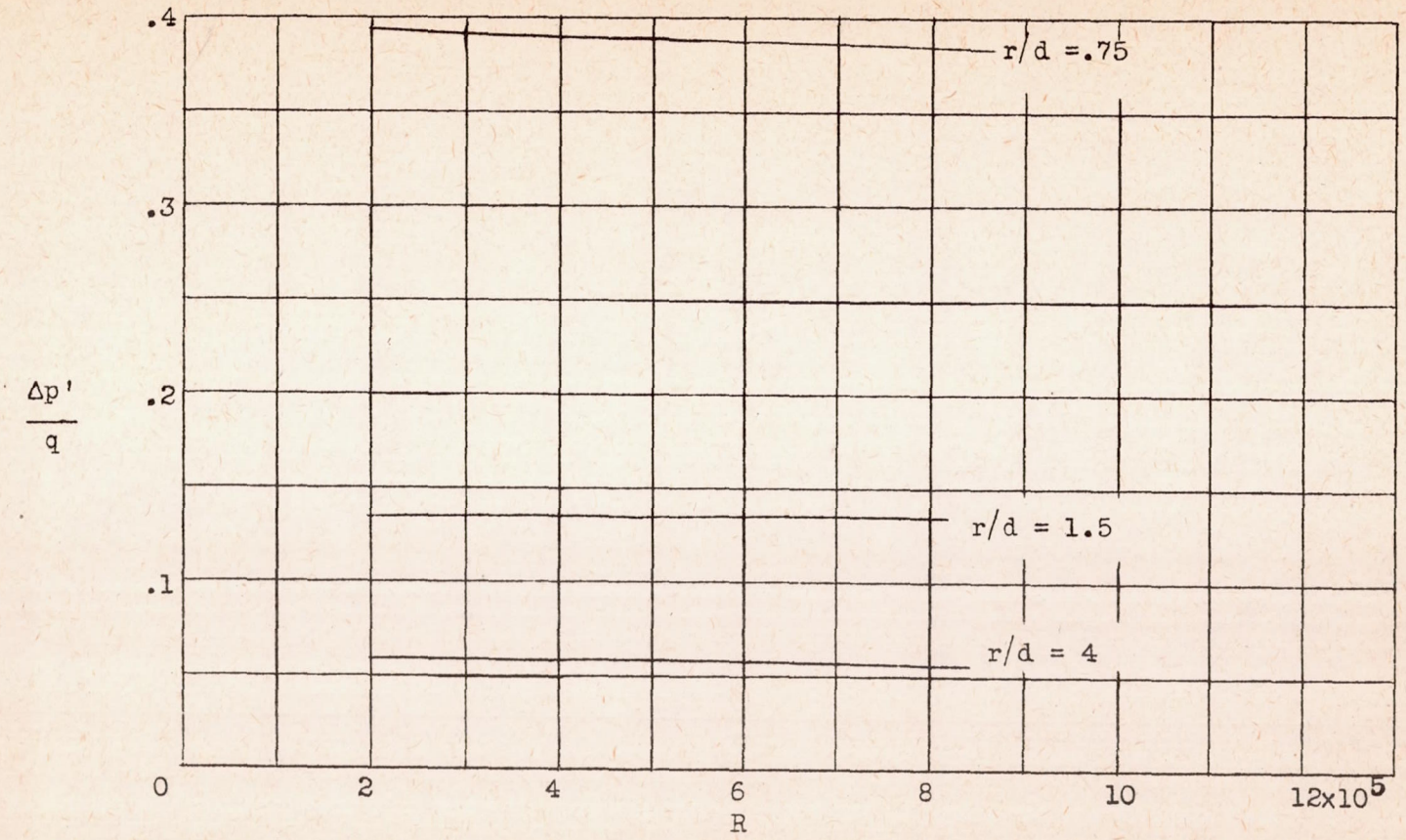

Figure 20.- Variation of net pressure drop with Reynolds number for single bends in square ducts.

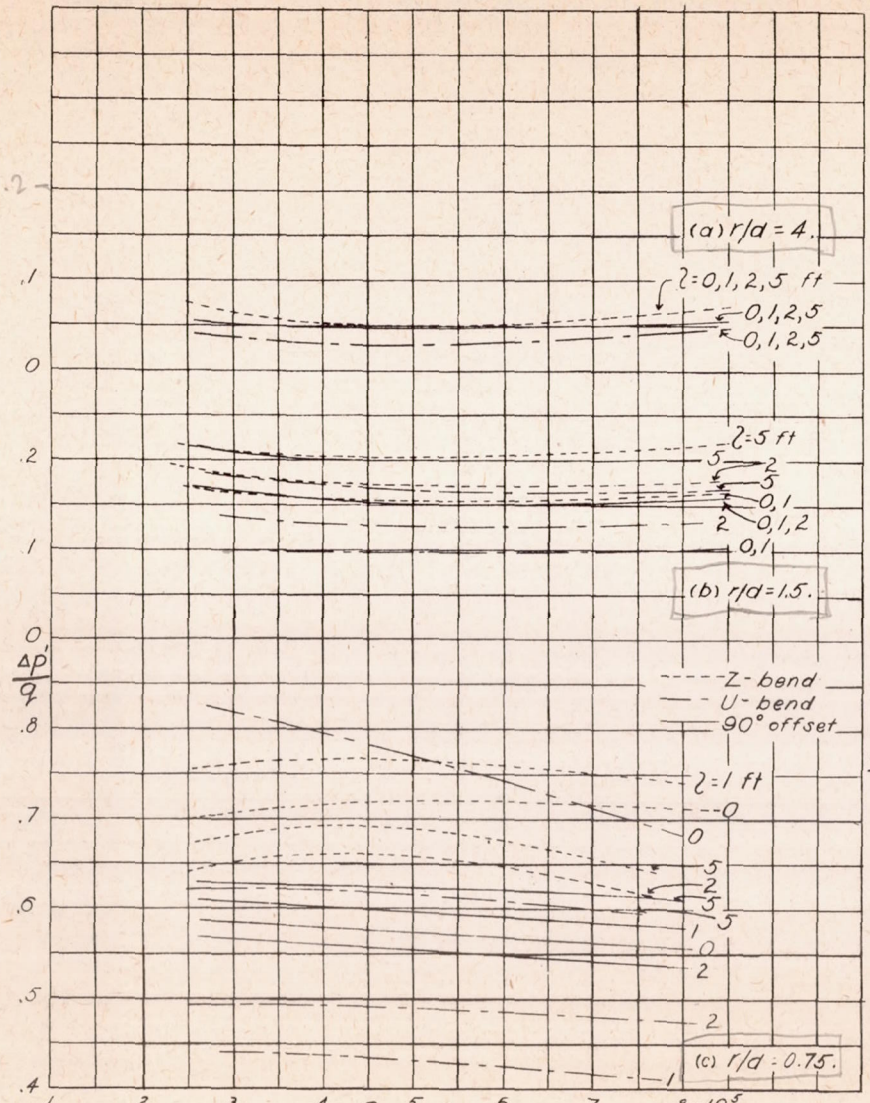

Figure 21.— Variation of net pressure drop with Reynolds number for compound bends in square ducts.

(Measure with 1/20")

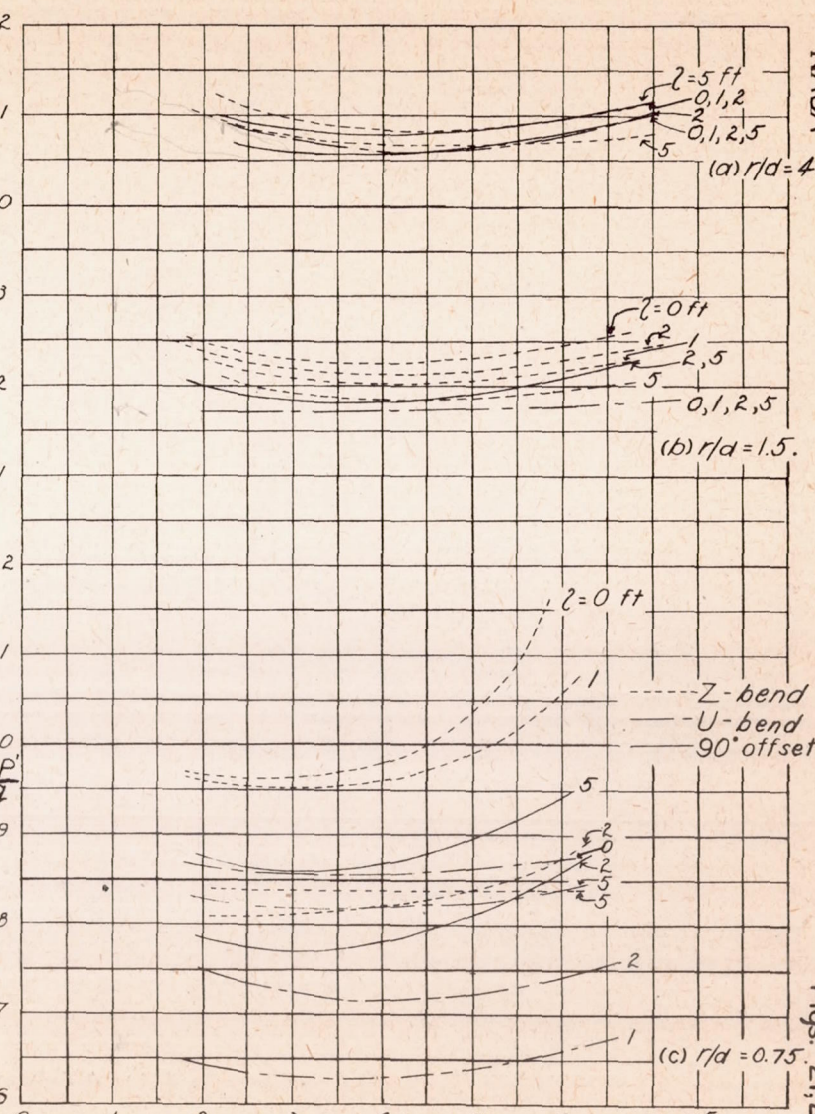

Figure 23.— Variation of net pressure drop with Reynolds number for compound bends in 3 by 1 rectangular ducts.

NACA

Figs. 21, 23

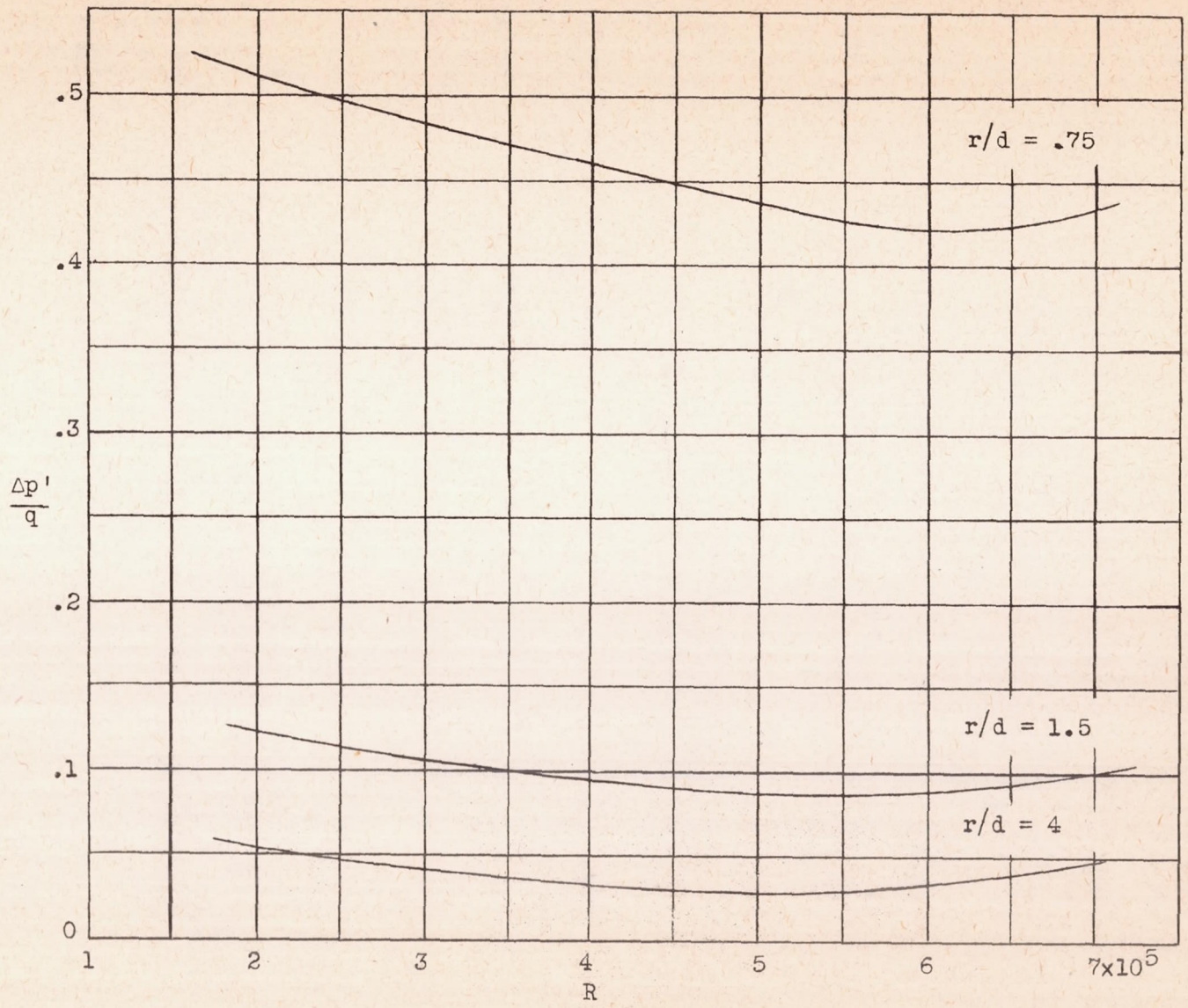

Figure 22.- Variation of net pressure drop with Reynolds number for single bends in 3 by 1 rectangular ducts.

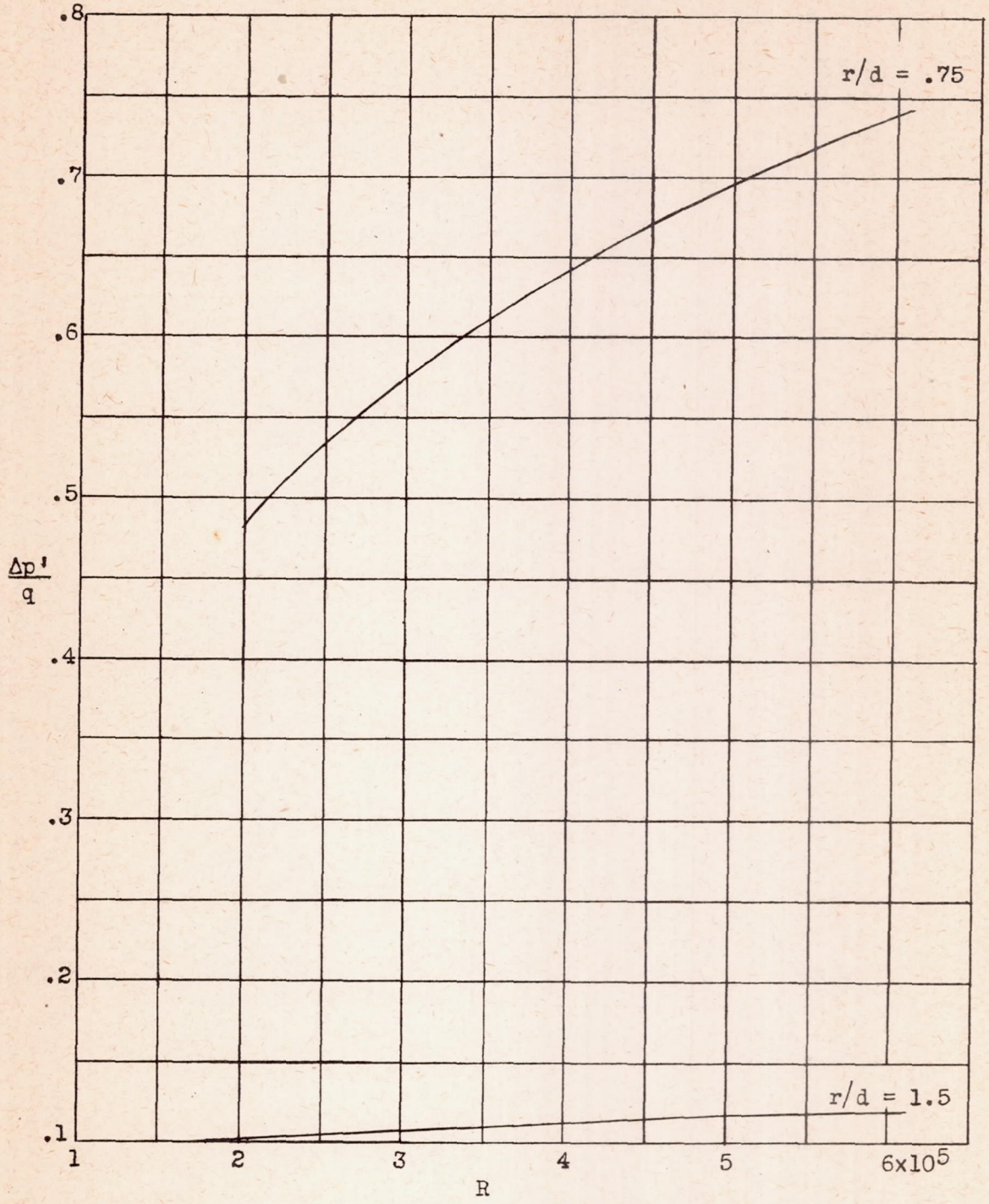

Figure 24.- Variation of net pressure drop with Reynolds number for single bends in 5 by 1 rectangular ducts.

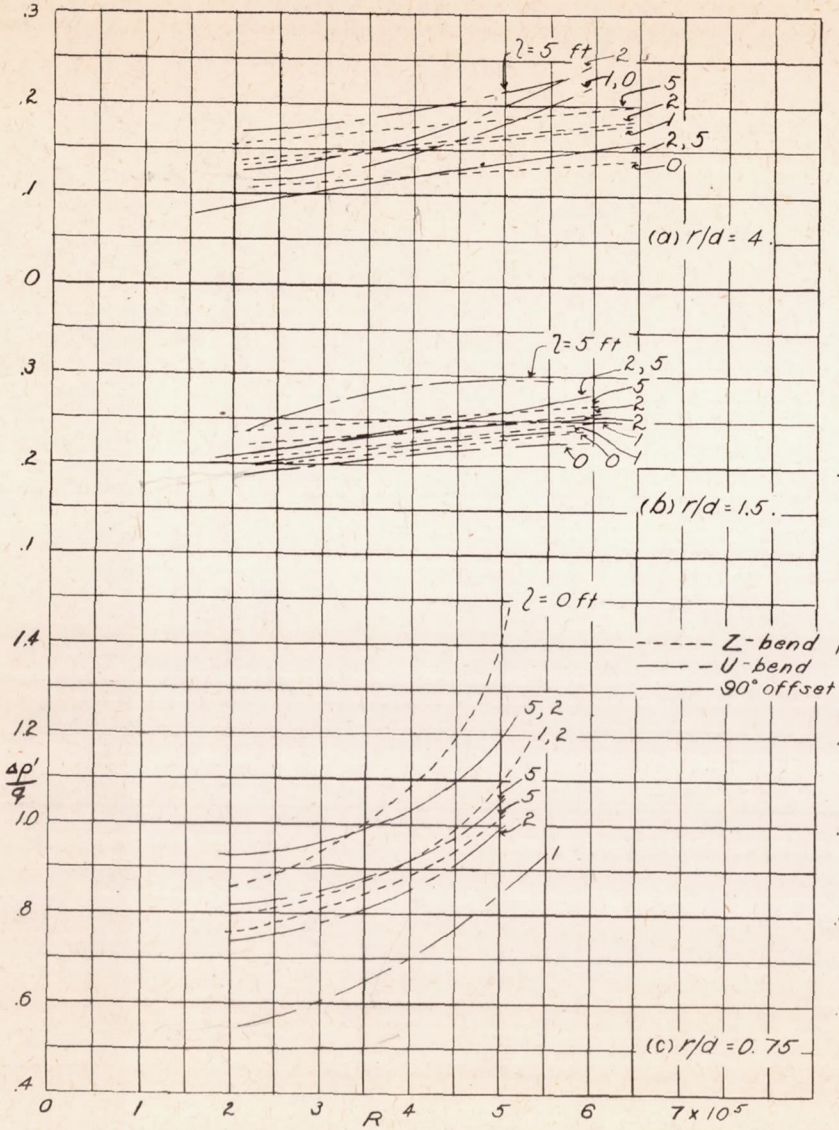

Figure 25.- Variation of net pressure drop with Reynolds number for compound bends in 5 by 1 rectangular ducts. (Measure with 1/20")

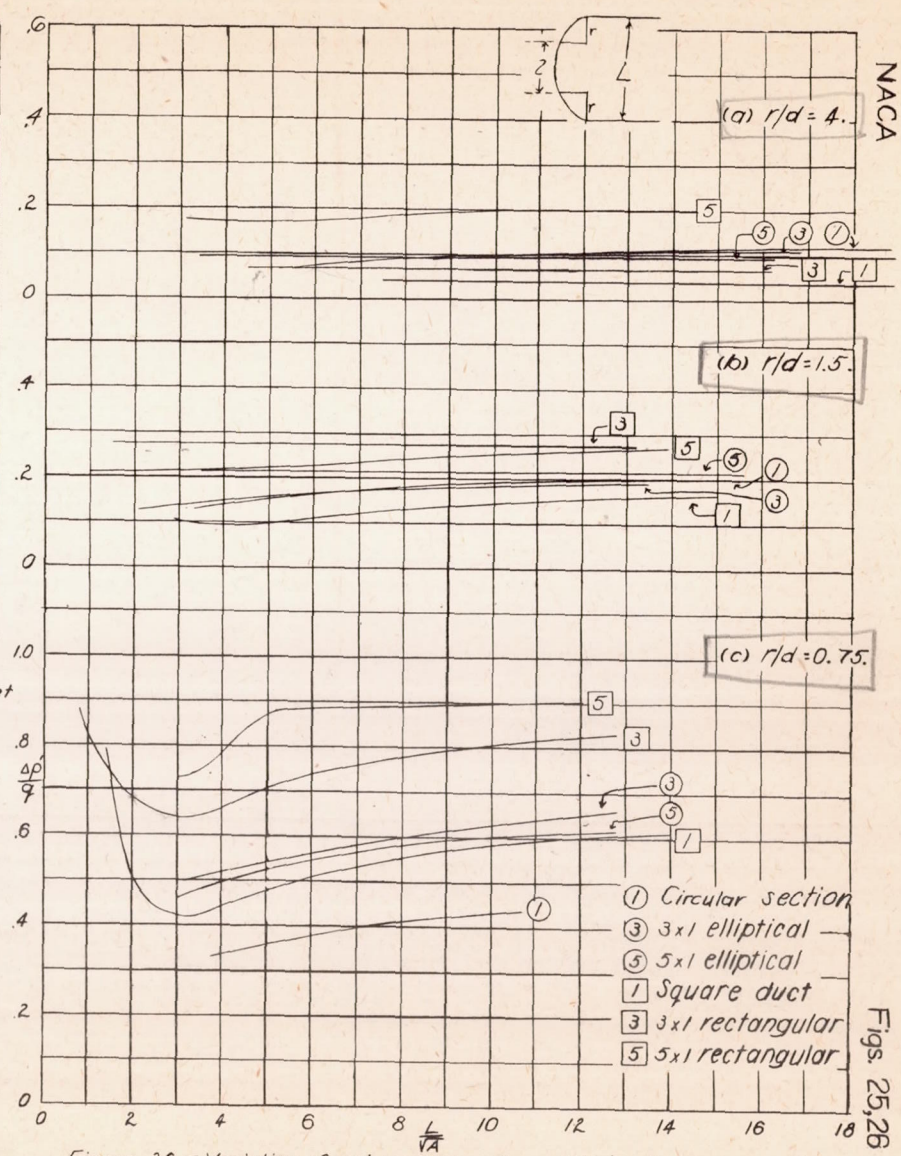

Figure 26.- Variation of net pressure drop with length of spacer for compound U-bends.

NACA

Figs. 25,26

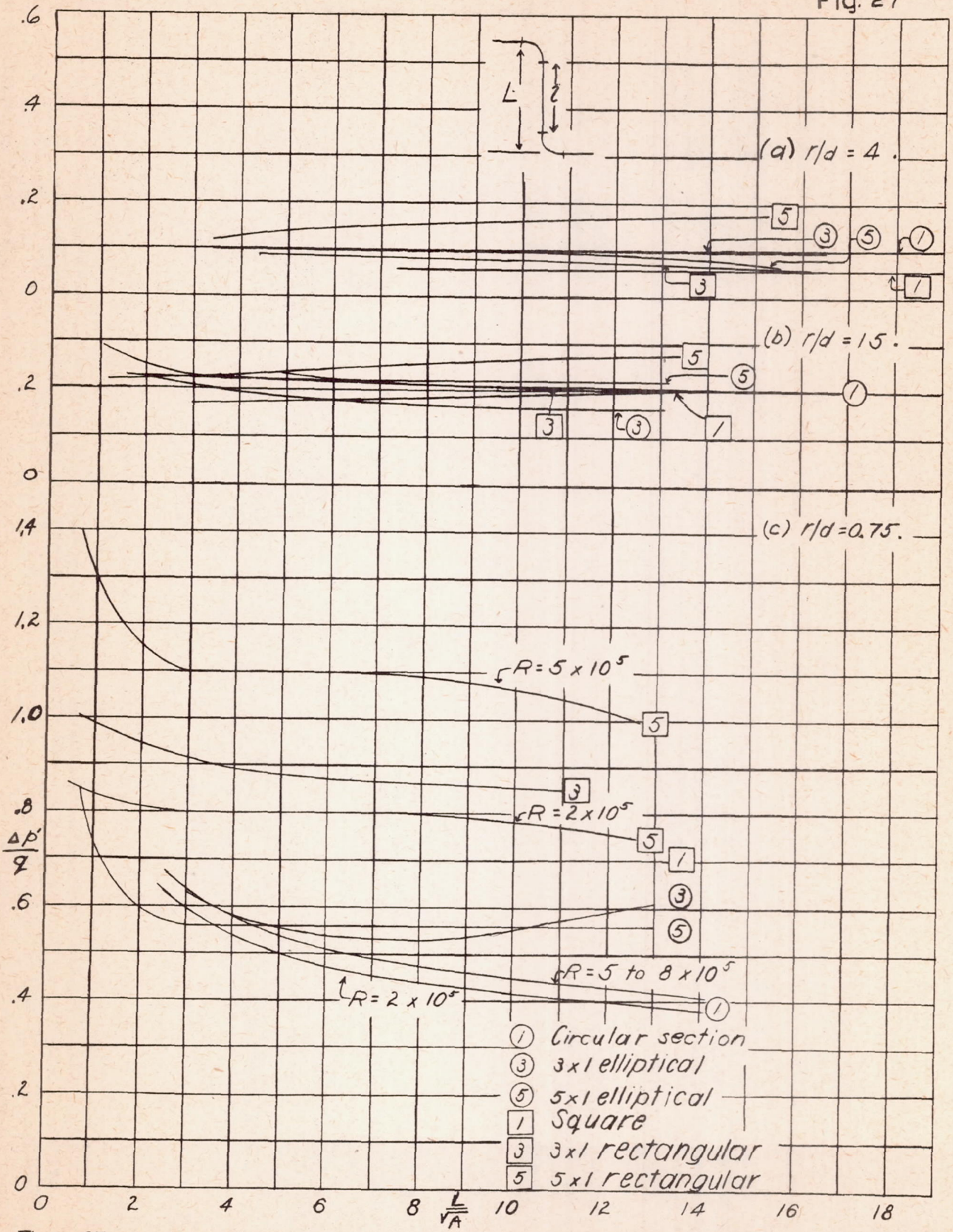

Figure 27.- Variation of net pressure drop with length of spacer for compound Z-bends. (Measure with 1/30")

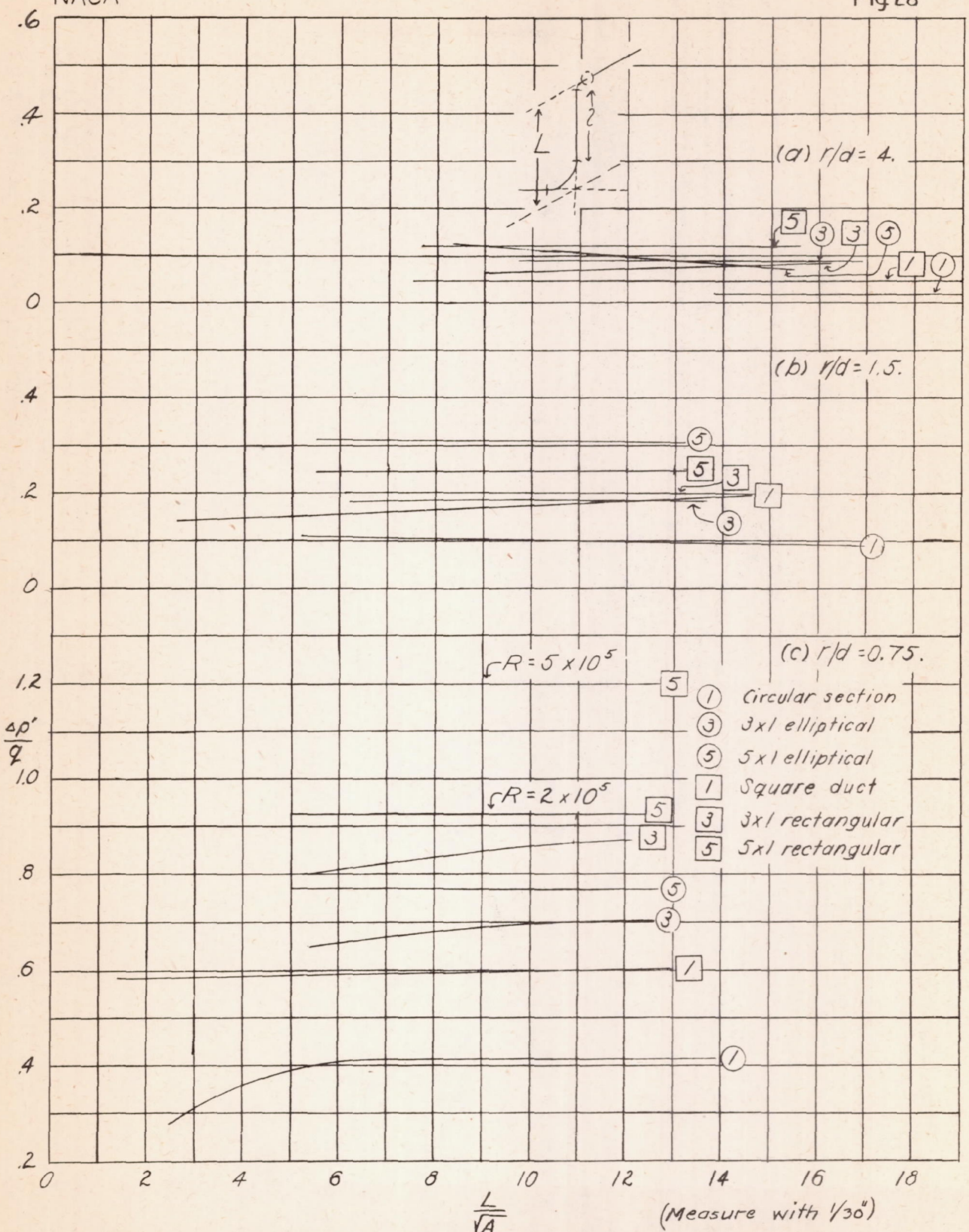

Figure 28.- Variation of net pressure drop with length of spacer for compound 90°-offset bends.

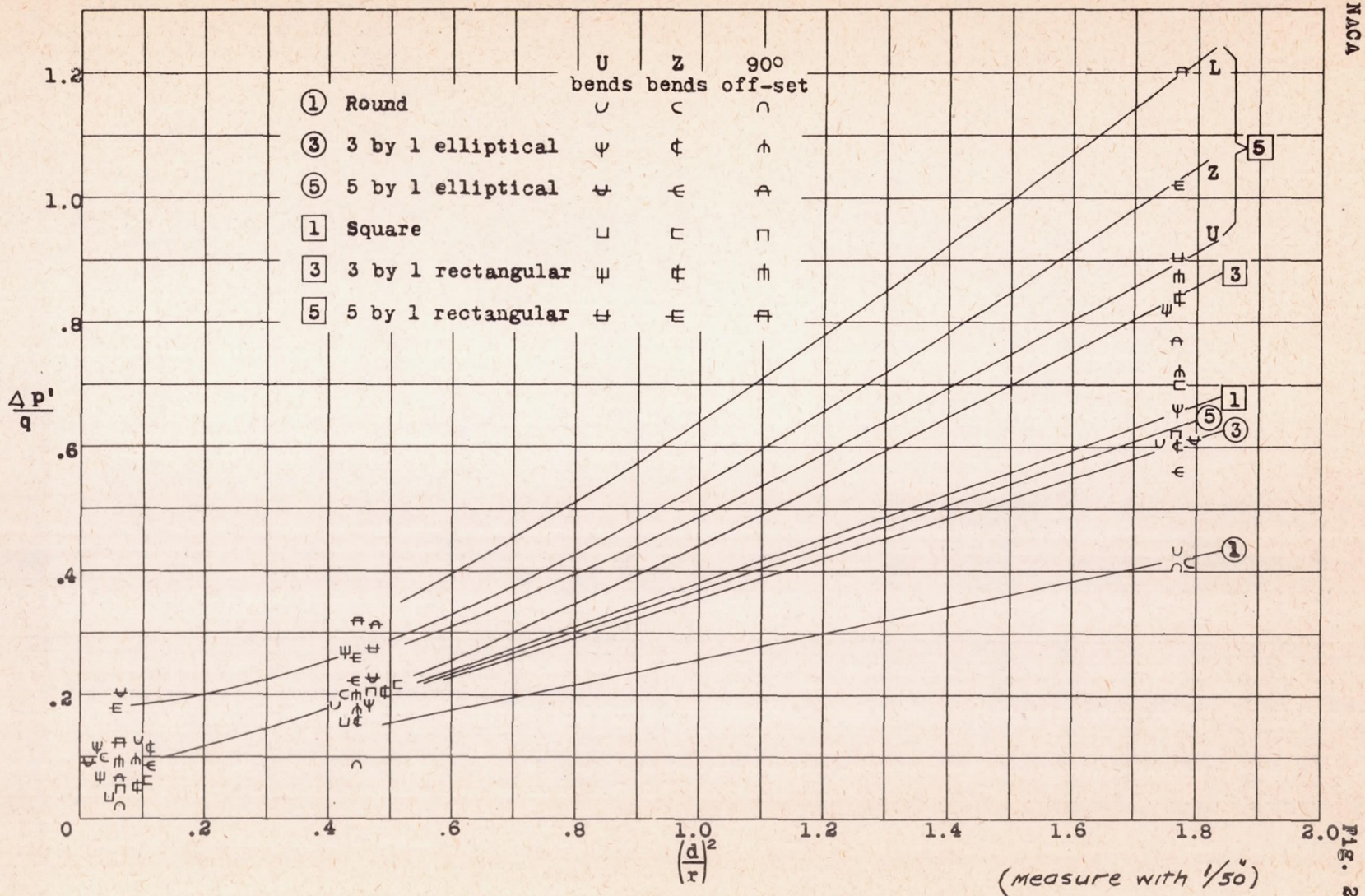

Figure 29.- Variation of net pressure drop with radius of curvature for compound bends with maximum spacer.

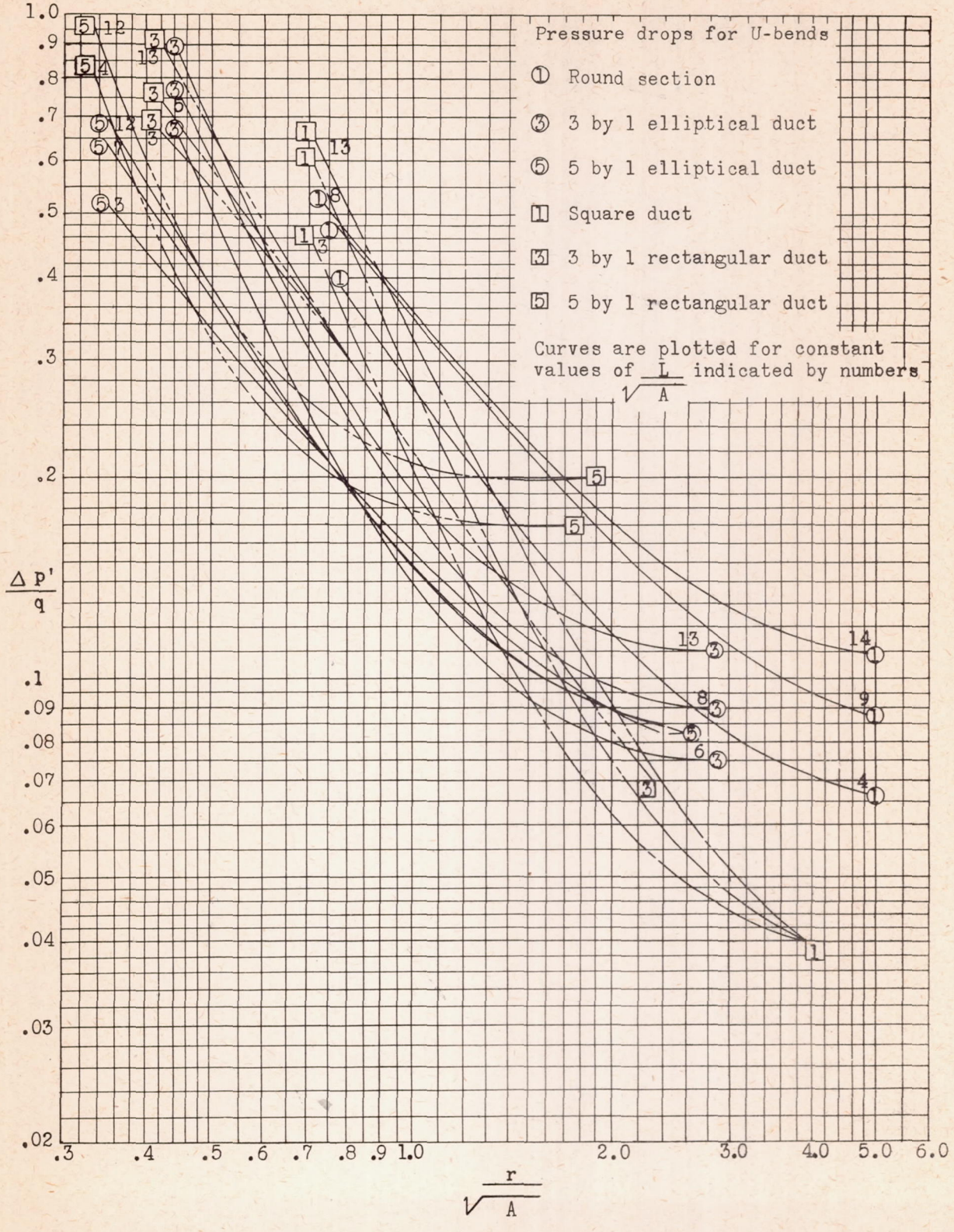

Figure 30.- Net pressure drop against radius of curvature for U-bends.

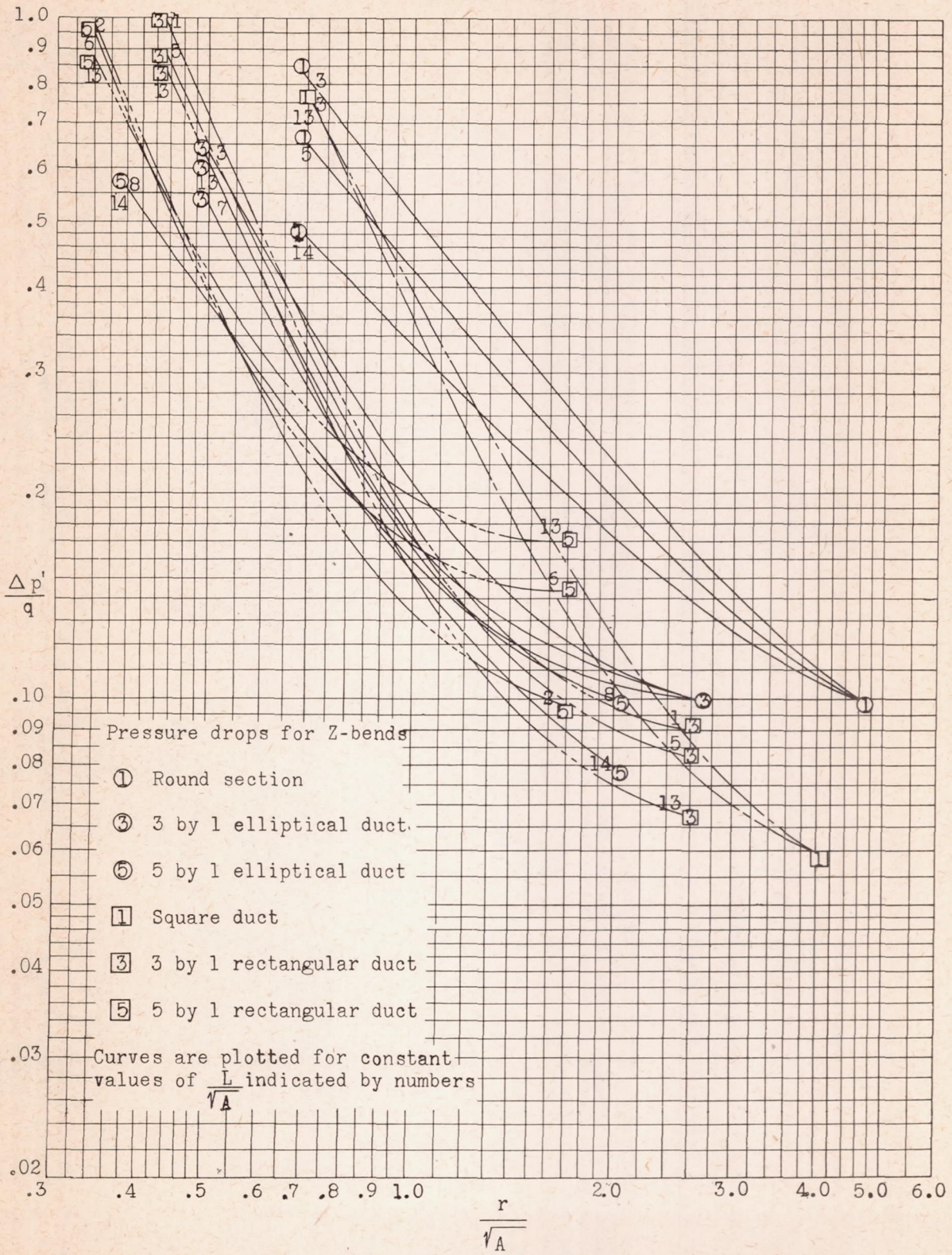

Figure 31.—Net pressure drop against radius of curvature for Z-bends.

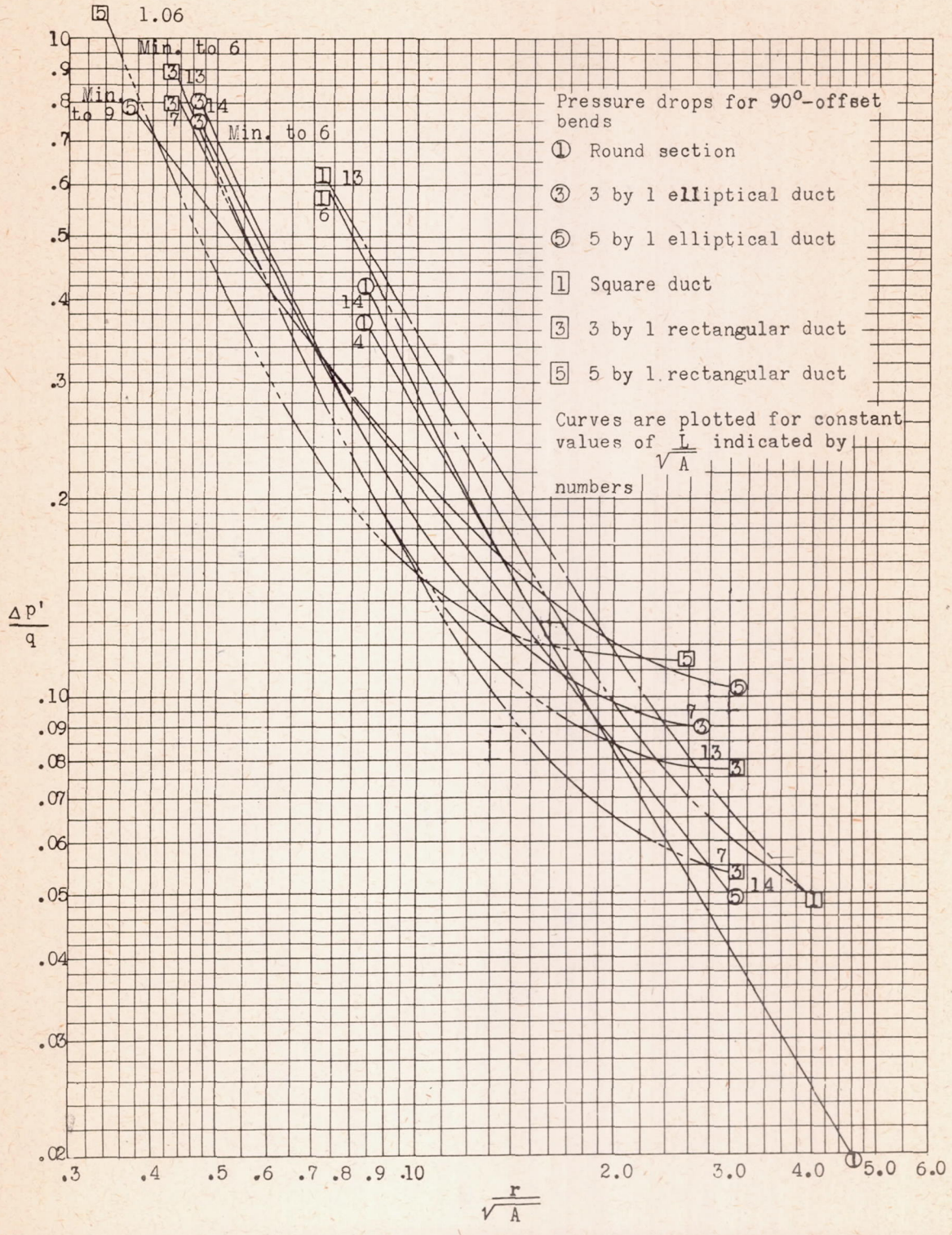

Figure 32.- Net pressure drop against radius of curvature for 90°-offset bends.

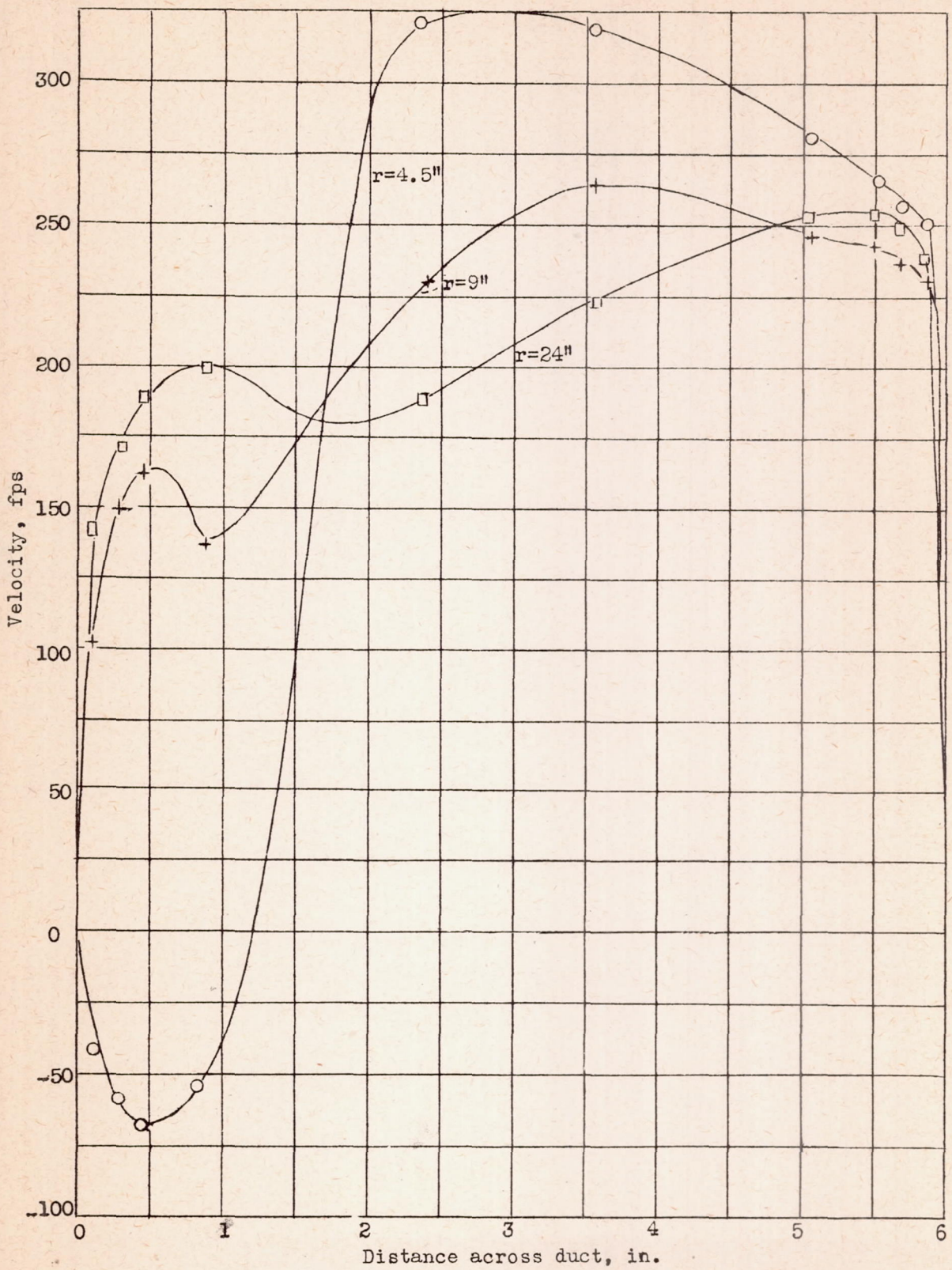

Figure 33.- Velocity distribution downstream of single elbow in plane of curvature.

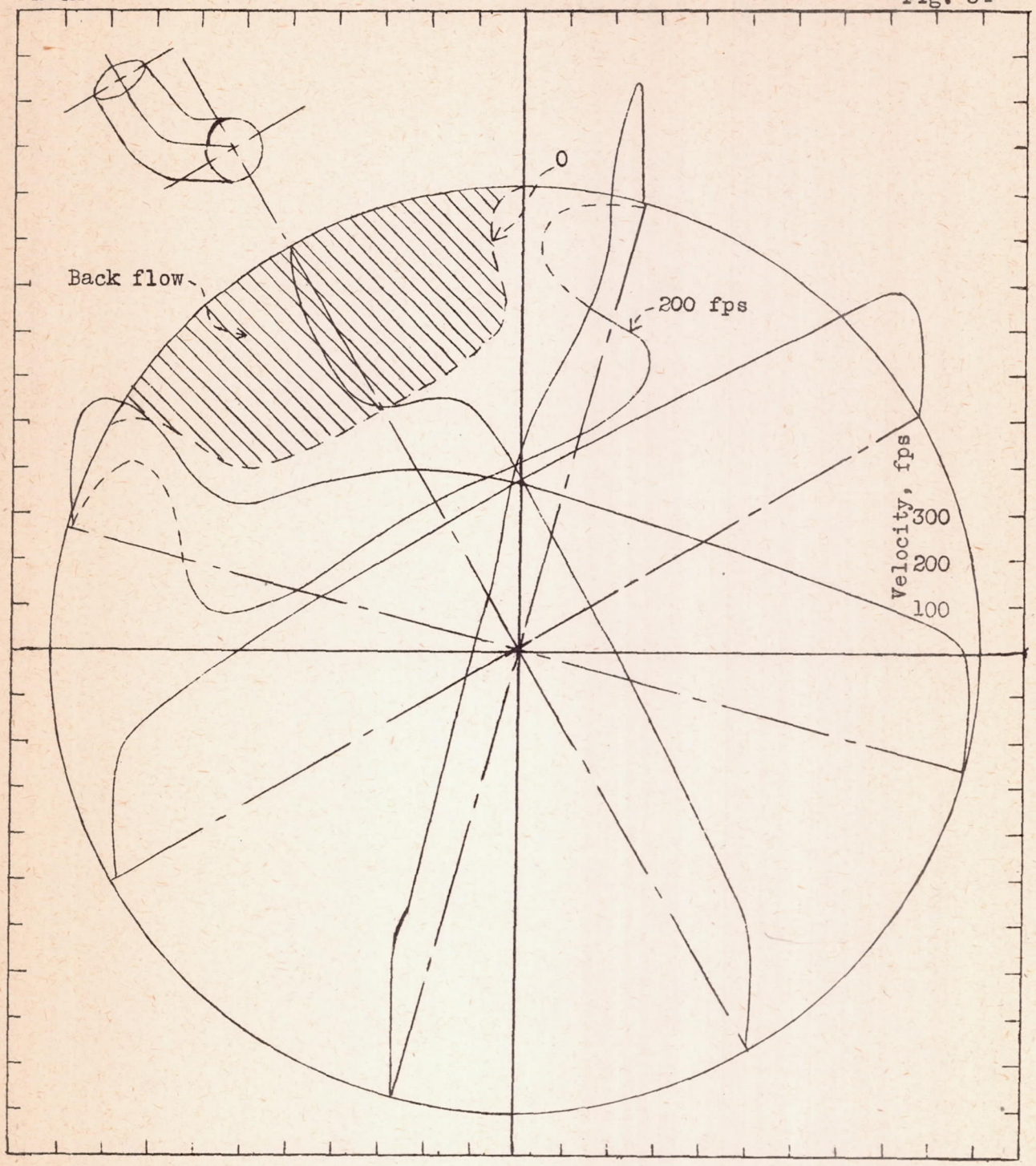

Figure 34.- Velocity traverses and constant-velocity contours at outlet of 4-1/2-inch-radius single elbow.

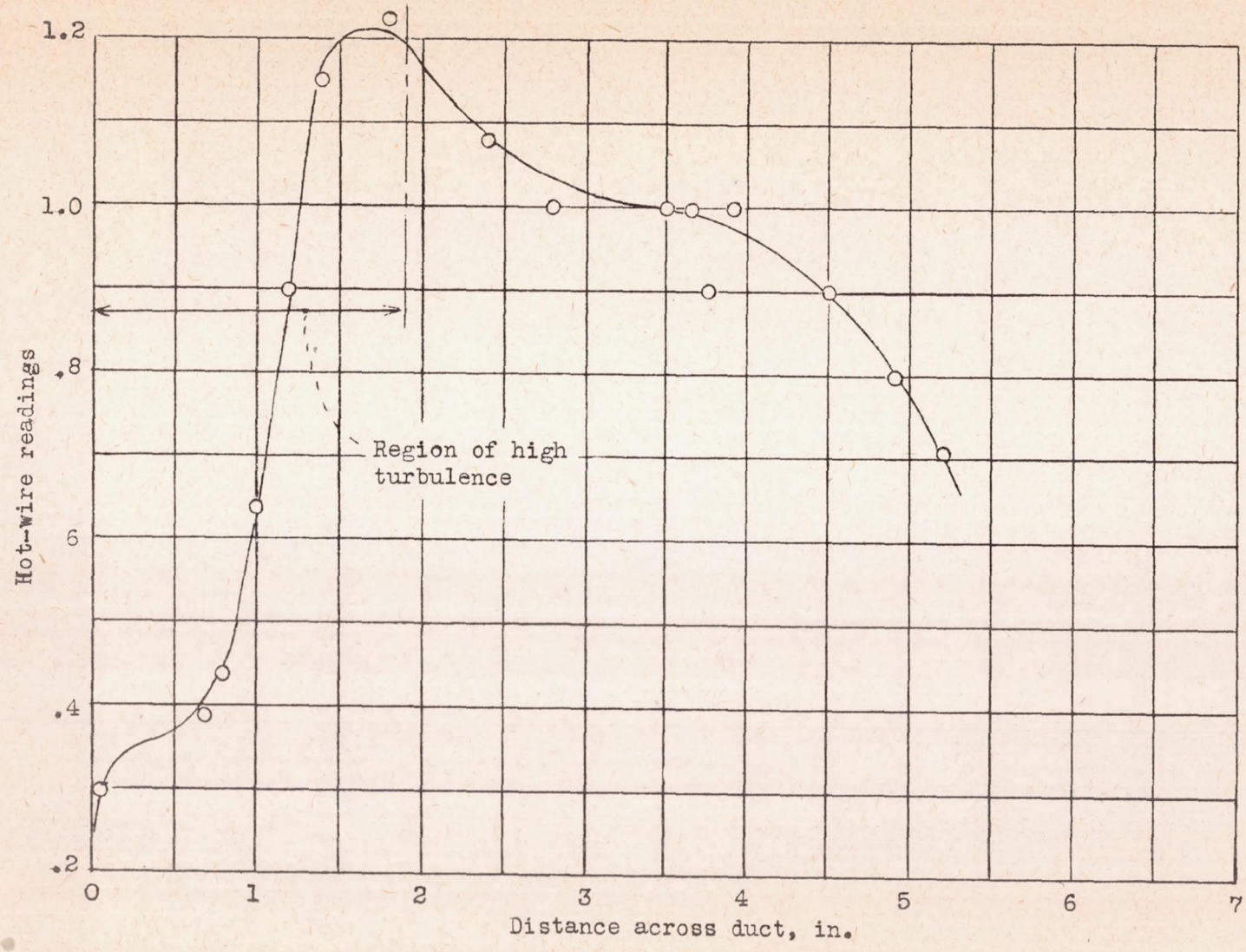

Figure 35.- Hot-wire traverse in the plane of curvation downstream of 4-1/2-inch-radius single elbow.

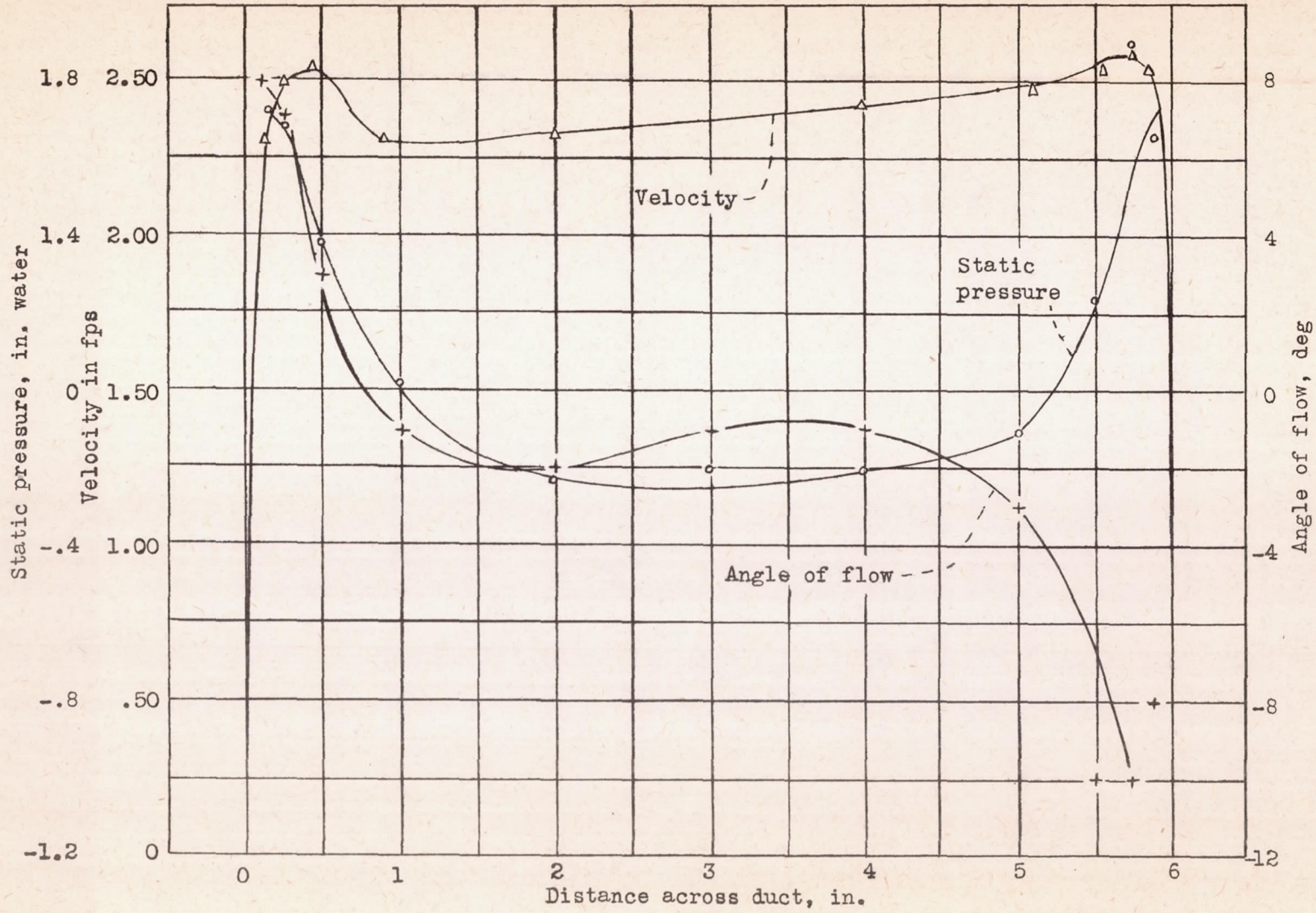

Figure 37.- Surveys at outlet of 90°-offset bend; r = 9 inches; line of survey normal to plane of second elbow.